

Isak Bernhard Elias Myhr Lamvik
Marius Lunder Jensen

Design-for-disassembly solutions for longitudinal joint connections in hollow core floors

Master's thesis in Civil and Environmental Engineering

Supervisor: Vegard Alme Ulstein

Co-supervisor: Øystein Rønningen

June 2023

Isak Bernhard Elias Myhr Lamvik
Marius Lunder Jensen

Design-for-disassembly solutions for longitudinal joint connections in hollow core floors

Master's thesis in Civil and Environmental Engineering
Supervisor: Vegard Alme Ulstein
Co-supervisor: Øystein Rønningen
June 2023

Norwegian University of Science and Technology
Faculty of Engineering
Department of Structural Engineering





MASTER THESIS 2023

SUBJECT AREA: CONCRETE STRUCTURES	DATE: June 8, 2023	NO. OF PAGES: 70 (thesis) + 4 (Appendix)
--------------------------------------	-----------------------	---

TITLE:

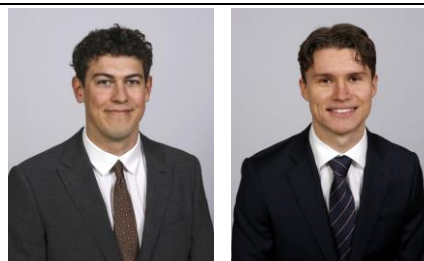
Design-for-disassembly solutions for longitudinal joint connections in hollow core floors

Prosjektering for demonterbare løsninger i langsgående fuger i hulldekketgulv

BY:

Isak Bernhard Elias Myhr Lamvik

Marius Lunder Jensen



SUMMARY:

The increasing demand for a more environmentally friendly construction industry has resulted in a focus towards the reuse of building elements. To facilitate better opportunities for reuse, it is necessary to establish innovative solutions for the connecting joints between these elements. A specific challenge arises with the adhesion between hollow core slabs and the longitudinal concrete joints that connect them together. Currently, removing joints with strong adhesion requires time-consuming procedures like drilling and sawing. However, applying separating actions on the surface of hollow core slabs prior to joint casting reduces adhesion, resulting in a significantly simplified disassembly process.

Two laboratory experiments were conducted to determine appropriate separating actions and their respective shear capacity. Firstly, separating actions were applied on cut-off hollow core slabs prior to casting. To evaluate adhesion, weights were dropped onto the joints, simulating the current practical disassembly process. Secondly, the separating actions exhibiting the least adhesion were applied to new concrete specimens tested to evaluate their shear capacity. A variable force was applied to the HCS, while a support was positioned under the grouted joint with minimal eccentricity to minimize contributions from bending moments. The tests were conducted with a constant compression force transverse to the joint. The output was a shear-slip relationship for each separating action.

The revised version of EC2 removes the limit for the maximum average shear stress in longitudinal joints, as well as the contribution from adhesion. Consequently, the calculation of shear capacity relies on frictional transfer. According to the results, the separating actions with the highest fluidity retain the frictional effects caused by aggregate interlock to the greatest extent. Hence, Mapeform W100, an easy-flowing liquid, demonstrated the highest shear capacity while minimizing adhesion. As a result, the shear capacity reached adequate values within the requirements of EC2. In contrast, the thicker oils partly cover the irregularities of the concrete surface, reducing the shear capacity from friction.

The adhesion exhibited in certain specimens during the first experiment was remarkably strong. The significant variation in adhesion, in combination with an improved concrete joint quality, results in increased disassembly time. This emphasizes the risk undertaken by demolition contractors and highlights the need for solutions regarding design-for-disassembly (DfD).

RESPONSIBLE TEACHER: Assoc. Prof. Vegard Alme Ulstein

SUPERVISOR(S): Assoc. Prof. Vegard Alme Ulstein, Tech. Dir. Øystein Rønningen

CARRIED OUT AT: Department of structural engineering

Abstract

The increasing demand for a more environmentally friendly construction industry has resulted in a focus towards the reuse of building elements. To facilitate better opportunities for reuse, it is necessary to establish innovative solutions for the connecting joints between these elements. A specific challenge arises with the adhesion between hollow core slabs and the longitudinal concrete joints that connect them together. Currently, removing joints with strong adhesion requires time-consuming procedures like drilling and sawing. However, applying separating actions on the surface of hollow core slabs prior to joint casting reduces adhesion, resulting in a significantly simplified disassembly process.

Two laboratory experiments were conducted to determine appropriate separating actions and their respective shear capacity. Firstly, separating actions were applied on cut-off hollow core slabs prior to casting. To evaluate adhesion, weights were dropped onto the joints, simulating the current practical disassembly process. Secondly, the separating actions exhibiting the least adhesion were applied to new concrete specimens tested to evaluate their shear capacity. A variable force was applied to the HCS, while a support was positioned under the grouted joint with minimal eccentricity to minimize contributions from bending moments. The tests were conducted with a constant compression force transverse to the joint. The output was a shear-slip relationship for each separating action.

The revised version of EC2 removes the limit for the maximum average shear stress in longitudinal joints, as well as the contribution from adhesion. Consequently, the calculation of shear capacity relies on frictional transfer. According to the results, the separating actions with the highest fluidity retain the frictional effects caused by aggregate interlock to the greatest extent. Hence, Mapeform W100, an easy-flowing liquid, demonstrated the highest shear capacity while minimizing adhesion. As a result, the shear capacity reached adequate values within the requirements of EC2. In contrast, the thicker oils partly cover the irregularities of the concrete surface, reducing the shear capacity from friction.

The adhesion exhibited in certain specimens during the first experiment was remarkably strong. The significant variation in adhesion, in combination with an improved concrete joint quality, results in increased disassembly time. This emphasizes the risk undertaken by demolition contractors and highlights the need for solutions regarding design-for-disassembly (DfD).

Sammendrag

De økte kravene til en mer miljøvennlig byggebransje har resultert i økt fokus på ombruk av byggeelementer. For å legge til rette for ombruk, er det nødvendig å etablere innovative løsninger for knutepunktene mellom disse elementene. En av hovedutfordringene er knyttet til heften mellom hulldekkene og de langsgående betongfugene som kobler dekket sammen. I dagens riveprosesser er fjerningen av betongfugen utfordrende, og tidkrevende tiltak som drilling og saging er nødvendig. Påføring av separerende tiltak som forskalingsolje på sidekant av hulldekke før fugestøp kan redusere heften betydelig, og dermed forenkle demonteringsprosessen.

To laboratorieeksperimenter ble utført for å finne fordelaktige separerende tiltak, samt deres respektive skjærkapasiteter. I det første eksperimentet ble separerende tiltak påført utskjærte prøvestykker av hulldekke i forkant av fugestøp. For å fastslå heftbidraget ble vekter sluppet ned på fugen for å simulere dagens demonteringsprosess. Deretter ble de separerende tiltakene som reduserte heften mest påført på nye betongstykker for å teste deres skjærkapasitet. En varierende kraft ble påført hulldekket og opplageret ble plassert under fugebetongen med minimal eksentrisitet for å redusere momentbidraget til testen. Testene ble gjennomført med en konstant trykkraft normalt på fugen. Resultatet fra testen var et skjær-forskyvnings-forhold for hvert separerende tiltak.

Den reviderte versjonen av EC2 fjerner begrensningen for maksimal gjennomsnittlig skjærkapasitet i langsgående fuger, samt heftbidraget. Som et resultat er beregninger av skjærkapasitet kun avhengig av bidrag fra friksjonseffekter. Resultatene viser at de separerende tiltakene med høyest fluiditet i størst grad beholder friksjonsegenskapene i form av "aggregat interlock" best. Derfor hadde W100, en tyntflytende væske, den høyeste skjærkapasiteten samtidig som heften ble minimert. Løsningen hadde tilstrekkelig styrke i henhold til kravene i EC2. Til forskjell dekker de tykkere oljene delvis over ujevnheter i betongoverflaten, og reduserer dermed friksjonsbidraget.

Heften som ble observert i enkelte tester i det første eksperimentet var bemerkelsesverdig sterk. Den betydelige variasjonen i heft, samt økt kvalitet på fugebetongen fører til økt demonteringstid. Dette fremhever risikoen demonteringsentreprenører har, samt viktigheten av nye løsninger knyttet til projektering med tanke på demontering (DfD).

Preface

This Master's thesis was conducted at the Department of Structural Engineering at NTNU Trondheim, as part of the Civil and Environmental Engineering study program. The thesis, identified by the subject code TKT4950, carries 30 credits.

We would like to thank our supervisor, Assoc. Prof. Vegard Alme Ulstein, for providing continuous support and knowledge throughout the entire process. We would also like to express our appreciation to the laboratory personnel at the Laboratory for Material Technology at NTNU Trondheim, particularly Thomas Uhlving and Kåre Brottveit Olsby, for their assistance and patience during the laboratory experiments.

Furthermore, we are grateful for the contribution from Spenncon AS led by our co-supervisor Øystein Rønningen and the SirkBygg initiative from Skanska for providing us with a challenging and captivating subject, aimed at developing a more sustainable and green construction industry.

We extend our thanks to Øst-Riv AS, for inviting us to their demolishing site and providing us with valuable knowledge regarding the disassembly process. Additionally, we would like to thank Masters Builders Solutions and Mapei AS for their assistance in identifying suitable separating actions and promptly delivering them to us.

Lastly, we thank Betongelementforeningen for inviting us to the conference Betongindustridagene 2023, where we had the opportunity to engage with a wide range of engineers from the industry.

Definitions

Abbreviations Throughout this master's thesis, the following abbreviations have been used consistently:

Eurocode 2	EC2
Betongelementboka	BEB
The International Federation for Structural Concrete	fib
Hollow Core Slab(s)	HCS
Design for disassembly	DfD

Contents

Abstract	i
Sammendrag	ii
Preface	iii
Definitions	iv
Table of contents	vii
1 Introduction	1
1.1 Motivation	1
1.2 SirkBygg Project	2
1.3 Taxonomy in construction and infrastructure industry	2
2 Theory	4
2.1 Hollow core slabs	4
2.2 Plate and plane structure systems	5
2.3 Vertical shear transfer between HCS	6
2.4 Dimensioning shear forces in monolithic floor systems of HCS	7
2.5 Friction	12
2.6 Compressive forces due to transverse steel	14
2.7 Design shear capacity in connections with concrete-to-concrete interfaces	16
2.8 Upper limit for the shear capacity	19
2.9 Joint assembly	20
3 Previous studies	21
3.1 Walraven and Reinhardt 1981	21
3.2 Composite concrete-to-concrete bond	21
3.3 Various research applications with potential relevance	24

4	Disassembly process of HCS today	27
4.1	The disassembly process	27
4.2	Topics regarding today's disassembly process	30
5	Methodology	33
5.1	First laboratory experiment; shear stress transfer Separating actions	33
5.1.1	Test components and material properties	34
5.1.2	Test setup	35
5.1.3	Collection of data	36
5.1.4	Sources of error	37
5.2	Second laboratory experiment; shear stress transfer	38
5.2.1	Test components and material properties	39
5.2.2	Test setup	40
5.2.3	Collection of data	43
5.2.4	Data processing	44
5.2.5	Sources of error	44
6	Results	45
6.1	First laboratory test; adhesion test	45
6.1.1	Concrete properties	45
6.1.2	Grading of adhesion	46
6.2	Second laboratory experiment; shear capacity	47
6.2.1	Dry	47
6.2.2	MasterFinish FW324	49
6.2.3	Olive Oil	50
6.2.4	MasterFinish RL224	51
6.2.5	Mapeform W100	52
6.2.6	Results and material properties	53

7 Discussion	56
7.1 Concrete properties	56
7.2 Capacity	56
7.3 Determination of the contribution from adhesion and friction	58
7.4 Shear slip relation	59
7.5 Normal compression forces in the longitudinal joint	60
7.6 Challenges for reuse	60
7.6.1 Adhesion	60
7.6.2 Logistics	61
7.7 Determination of the best separating action	62
7.8 Sources of error from the results	63
8 Conclusion and future work	65
8.1 Conclusion	65
8.2 Future work	66
8.2.1 External variables	66
8.2.2 Laboratory experiment without normal stress	66
Bibliography	68
Appendix	71
A Pictures and descriptions from first laboratory test	71

1 Introduction

The demand for reuse of building elements is increasing to reduce the CO₂ emissions from the construction industry. Reuse of building elements requires different techniques and processes than traditional demolition followed by constructing a new building with new materials. Today, this process is neither efficient nor economically sustainable. Therefore, new solutions regarding deconstruction, transport, verification, and rebuilding are required to develop the construction industry.

Hollow core slabs, hereby called HCS, are easy to reuse due to their standardized geometry, which will be discussed in detail later. One of the key challenges in the deconstruction of HCS is the removal of concrete grouted in the longitudinal joints. The joint concrete has a variable level of adhesion to the HCS, which sometimes requires drilling, chiselling, and sawing in order to split and remove the joint concrete. The variation of adhesion is experienced by construction workers, stating a large variation of time consumed to remove the HCS [1]. While some projects have seen effective and predictable deconstruction processes, others have required time-consuming tasks. This variability makes time estimation for HCS deconstruction challenging and increases the risk of cost calculations. Factors such as contamination of the HCS before casting, as well as the quality of the joint work, are believed to be significant for the adhesion between the elements.

As a result, it is essential to find solutions addressing the issue of varying adhesion that does not come at the expense of disassembly time. Therefore, this master's thesis focuses on studying ways of reducing the adhesion between grouted concrete joints and the surface of HCS. One potential solution is the use of separating actions such as formwork oils, which could effectively reduce adhesion. However, it is important to ensure that this reduction in adhesion does not compromise the shear capacity of the joint. Therefore, the two main objectives of this master's thesis are to identify separating actions that reduce adhesion in the joints, while still ensuring sufficient shear capacity.

1.1 Motivation

The Ellen MacArthur Foundation, which works with education and science linked to the circular economy and people's views on sustainability, emphasizes that technological advancements in energy sources used today only account for half of the necessary change to achieve a sustainable planet [2]. Regarding the construction industry, Ellen MacArthur presents strategies emphasising reuse and recycling, which the foundation believes will play a critical role. Constructing buildings with the end of lifespan in mind will simplify the disassembly process and the ability to reuse and recycle. In other words, this proactive way of constructing buildings will primarily gain its potential in the far future when the lifespan of the building is increased. Hence, the inception of an end-of-lifespan mindset in the construction industry needs to be introduced as soon as possible.

The perspective emphasized by The Ellen MacArthur Foundation serves to underscore the motivation behind this master's thesis. The aim is to formulate hypotheses, test them through experiments, bring in perspectives from current practical processes, and discuss the results based on accumulated experience, knowledge, analysis, and theory. This research will hopefully contribute to, and inspire further studies, assisting the construction industry in its pursuit of sustainable goals and fostering a more sustainable planet.

1.2 SirkBygg Project

This master's thesis is written in relation to SirkBygg, an initiative aimed at developing efficient and sustainable solutions for the reuse of buildings [3]. This master's thesis is related to the initiative through Spenncon AS, which works on finding rational, dismountable, and reusable solutions that facilitate a circular mindset and increase the lifespan of building elements. This practice is called design-for-disassembly, abbreviated as DfD, and focuses on designing solutions that are easy to deconstruct. The goal of the SirkBygg DfD-initiative is to reduce CO2 emissions by 90 % compared to traditional demolition and producing of new materials. Currently, a pilot project is underway at Helsefyr in Oslo. This project uses DfD-practices, utilizing simple methods and materials. This pilot project will increase the knowledge of reuse, and examine solutions for future practice. In essence, while the development of reuse technology has begun, there is still a substantial need for studies to explore effective design-phase solutions for connections.

1.3 Taxonomy in construction and infrastructure industry

Taxonomy, a system of classification, is one of the new areas of effort of the European Union (EU) with the aim of contributing to the choice of activities that can be defined as sustainable. The European Commission, the executive body of the European Union, started developing this taxonomy system in 2020 for sustainable finance by use of criteria for sustainable activities such as reuse, recycling, and low-carbon building materials [4][5]. To ensure the criteria are fulfilled, companies are imposed reporting- and publication requirements [5]. Fulfilling the criteria will lead to a gained advantage. The financial markets have an important impact on the transition to a more sustainable green economy, but there have been trends of different definitions of what is to be considered sustainable economic actions [6]. Therefore, the taxonomy has the purpose of forming a common understanding, which hopefully will lead to easier management of capital in the direction of green investment with classed positive sustainable impact. This will contribute, and possibly play a key role, to the fight against greenwashing. Particularly for Norway, a new law that legislates the EU taxonomy regulation (EU/2020/852) entered into force on January 1st 2023 [7]. The purpose of the law is to make sustainability information public in the financial sector. Finanstilsynet, the financial supervisory authority of Norway, is the authority that must make sure

the companies follow the law.

The taxonomy system is part of the European Green Deal, which is a set of policy initiatives by the European Commission with the goal for the EU to be climate neutral in 2050 [5][8]. The Green Deal covers several sustainability topics and different industries, but it aims to improve energy efficiency and reduce greenhouse gas emissions for the construction and infrastructure industry. This desired change shall be done through actions such as improving the environmental performance of buildings, supporting the development of sustainable building materials and technologies, and promoting sustainable public procurement.

BREEAM-NOR is the foremost environmental certification system for buildings in Norway and is built up so that points are obtained for green actions [9]. Fulfilling the criteria of taxonomy in The European Green Deal will also give points in the BREEAM-NOR-certification [6]. However, the BREEAM-NOR certification is based on the level of ambition and not the actual product. This is where the taxonomy has a stricter approach and thus sets absolute demands.

2 Theory

2.1 Hollow core slabs

Hollow core slabs (HCS) are precast concrete slabs with prestressed reinforcement, where the cross-section is constant over the length [10]. These slabs are cast mechanically at factories with a standard width of 1.2 meters [11]. HCS are characterized by their hollow channels, reducing weight while maintaining structural capacity. Depending on the demanded capacity of the element, the height available on the Norwegian market varies from 200 mm to 520 mm. The prestressed strands are embedded in the concrete. For a general overview of an HCS, see Figure 2.1. Hollow core slabs are generally used as flooring and roofs in infrastructure, residential, commercial and industrial constructions. To form floorings, the elements are connected with concrete cast in the joints.

The Norwegian BEB volume A ch. 6.2 provides some of the benefits of using HCS in structures [12]:

- It is possible to reach large deck spans relative to the height of the deck. Decks built up by HCS have a homogeneous smooth surface without supporting beams, which makes it easier to mount ventilation ducts and cable bridges. The hollow cores can also be used for ventilation channels. Additionally, the smooth surface reduces the need for ceiling panels.
- Use of prefabricated concrete elements, such as HCS, reduces construction and engineering time and ensures uniform quality of the concrete independent of climatic circumstances at the construction site. The assembly phase of the structure and facade is often a crucial factor for the overall timespan of a project. Prefabricated decks of HCS reduce the construction time significantly. Engineers also like to construct buildings of HCS due to its standardized and proven solutions, which reduce calculation time, while also increasing safety and reliability.

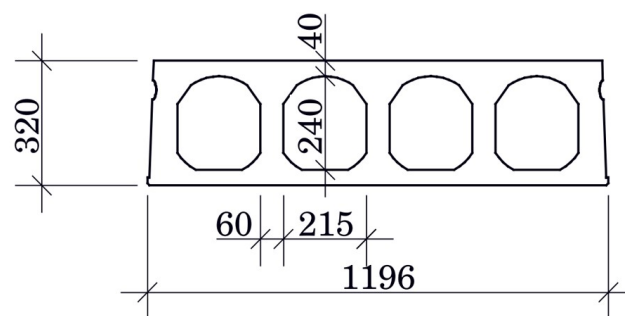


Figure 2.1: Geometry of a hollow core slab with height of 320 mm

HCS contains prestressed reinforcement in form of strands, which leads to an upward curvature of the floor as illustrated in Figure 2.2. Consequently, concrete topping is used to level the floor. When HCS is reused, the edge close to the transverse support is cut off. Depending on the adhesion

and thickness of the topping layer, the concrete topping is normally not removed. The topping remains on the element when installed into new structures. This issue will be discussed closer in Section 4.1 regarding the disassembly process.

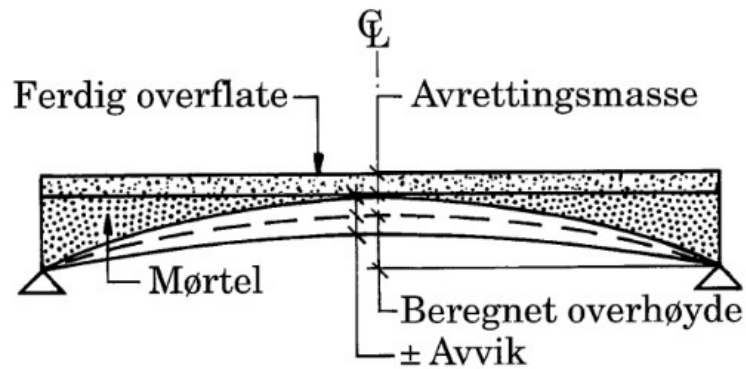


Figure 2.2: HCS with oversized curvature due to prestressing and concrete topping for levelling [12]

2.2 Plate and plane structure systems

This part is partially taken and translated from the project assignment of the course TKT4550 Construction Engineering Advanced Project [13].

Floor elements subjected to load in-plane and out-of-plane, are referred to as plane elements and plate elements respectively [14]. These two theoretical approaches are illustrated in Figure 2.3.

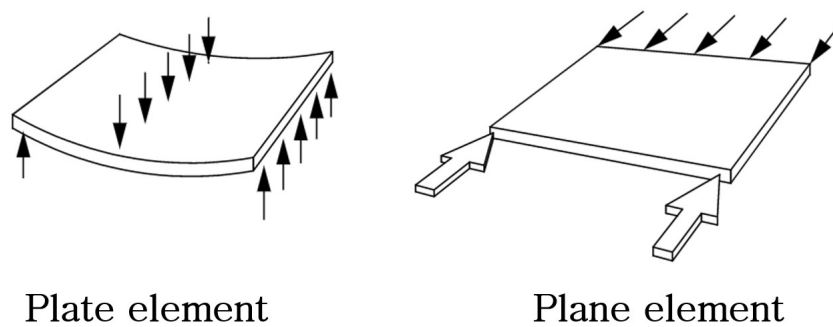


Figure 2.3: Illustration of a plane- and plate element [12]

If plane elements can transfer in-plane shear forces and bending moments between each other, the plane of HCS is referred to as monolithic systems or floor diaphragms in fib 2.3.1 [15]. The same counts for systems of plate elements which can transfer out-of-plane forces between each

other. For HCS, as described in BEB Volume B ch. 12.4.4, the forces need to be transferred by the concrete joints linking them together [12]. For structures where the floor behaves as a monolithic system, the lateral movements will be rigid body motions. Due to structures often being statically indeterminate, the relative stiffness will be decisive for the force distribution. This lateral rigid body motion is essential for the displacements to target the vertical-resisting elements. These vertical elements have high stiffness and are referred to as shear walls. The distribution and direction of shear walls are essential for the ability of the structure to resist lateral displacement. Figure 2.4 shows a structure with monolithic floor systems subjected to lateral displacement with shear walls on one side.

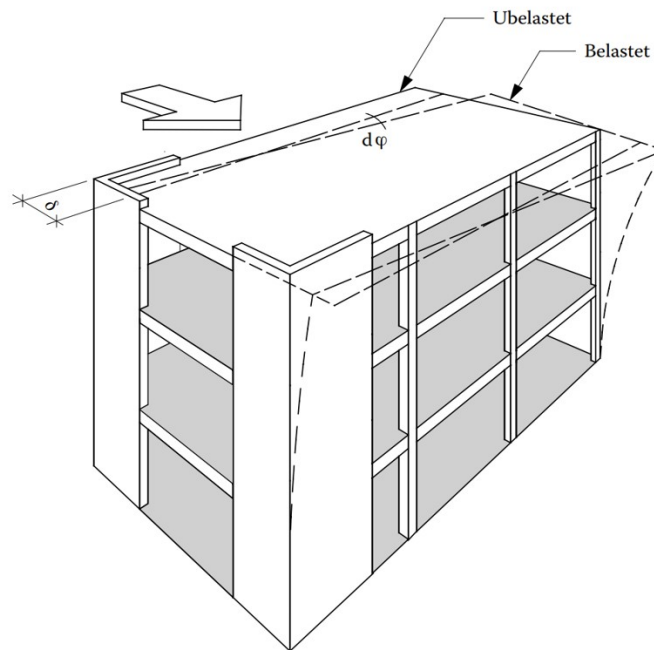


Figure 2.4: Structure with shear walls subjected to lateral displacement [12]

2.3 Vertical shear transfer between HCS

The longitudinal side surface on HCS has a beneficial design for transferring vertical shear forces due to teething in the vertical direction, as Figure 2.5 illustrates. According to fib 8.4.2.3, this teething is essential in order to transfer vertical shear within the joint. Subsequently, it is also claimed that cracking will occur when the connection is loaded in shear, and that shear forces will be transferred by an inclined compressive strut within the shear key. This compressive strut is also illustrated in Figure 2.5 and the clamping force H occurs to maintain equilibrium.

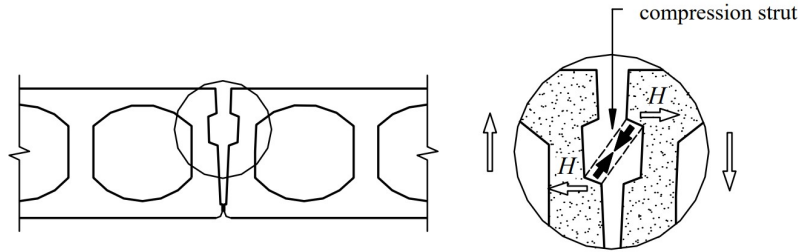


Figure 2.5: Cross section of the joint between HCS and vertical shear transfer in the toothed section of the joint [15]

2.4 Dimensioning shear forces in monolithic floor systems of HCS

This part is partially taken and translated from the project assignment in the course TKT4550 Construction Engineering Advanced Project [13].

Section 2.2 discussed the importance of shear transfer between HCS to have monolithic behaviour of floors. This section focuses on the dimensioning forces transferred by the concrete joint between HCS to sustain diaphragm action and how they arise from external lateral forces.

Monolithic rigid floors of HCS and shear walls subjected to lateral forces act similarly to a supported beam, as illustrated in Figure 2.6 from BEB volume B ch. 12.4.4. Figure 2.6 also contains the belonging bending moment- and shear diagram, which correlates with the force diagrams to a simply supported beam subjected to uniformly distributed vertical load. It can be observed that the maximum shear force occurs close to the supporting shear walls, and the maximum bending moment in the centre of the rigid floor.

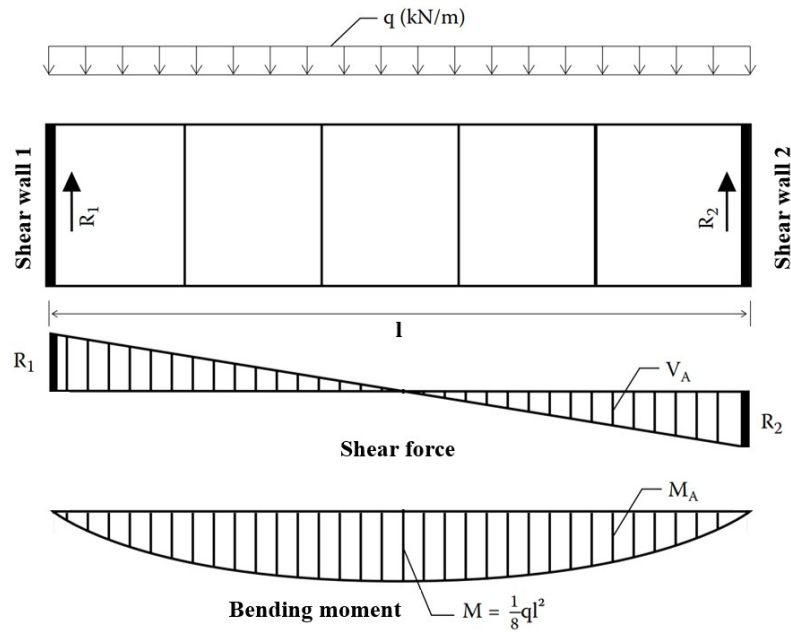


Figure 2.6: Monolithic floor of HCS subjected to lateral force with belonging shear- and bending moment diagram [12]

The internal moment arm, z , will differ from concrete beams in monolithic rigid floors of HCS due to the use of plane element theory instead of beam theory [14]. In a monolithic floor of HCS, where the transverse reinforcement is located at the edge, the effective height, d , is determined as the distance from the centre of reinforcement to the opposite edge of the concrete floor. BEB volume B ch. 12.4.2 [12] provides a scheme for finding the internal moment arm based on the different supports of plane concrete elements.

The first axis represents the distance between supports, or the distance to the edge of the cantilever, in ratio with the effective height, l/d or a/d . The second axis represents the ratio between the internal moment arm and the effective height, z/d . There is a convergence between the behaviour of the simply supported and cantilever elements, aligning with concrete beam theory where $z \approx 0.85d$ [16].

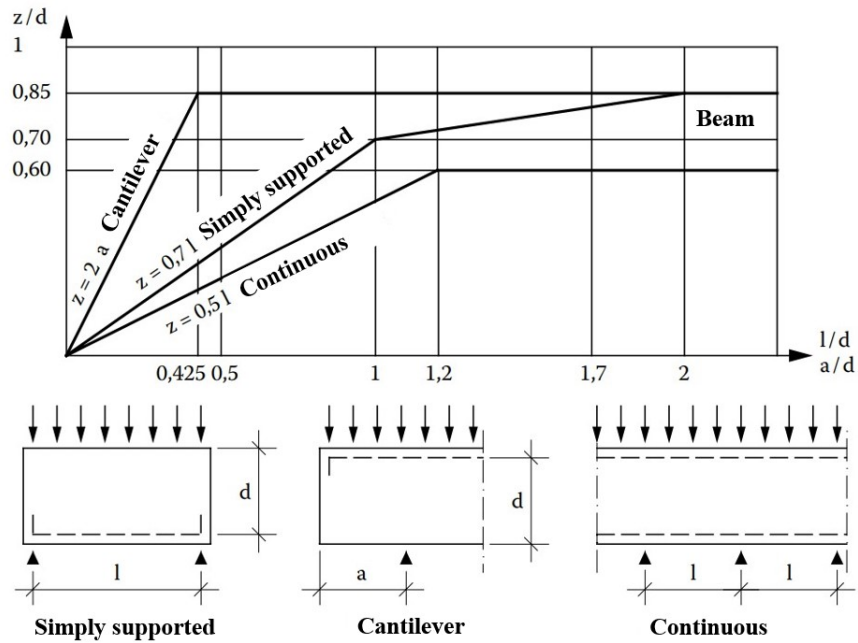


Figure 2.7: Internal moment arm [12]

With the internal moment arm, z , determined, it is possible to find the dimensioning stresses and strains of the monolithic concrete floor element subjected to external lateral forces. Figure 2.8 illustrates the possible stresses and strains acting in the plane along a cross-section of a monolithic concrete floor element. The internal moment arm determines the distance between maximum and minimum strains, and the distance between the compressive stress resultant and the tension stress resultant in the reinforcement. The shear stress is zero at the top, reaching its maximum at zero strain, and remains constant throughout the cross-section due to the tension caught up by the reinforcement.

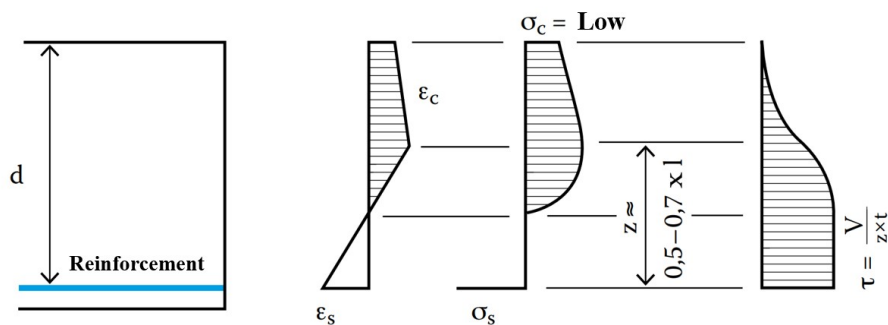


Figure 2.8: Stresses and strains in cross-section of monolithic concrete floor element subjected to external lateral forces [12]

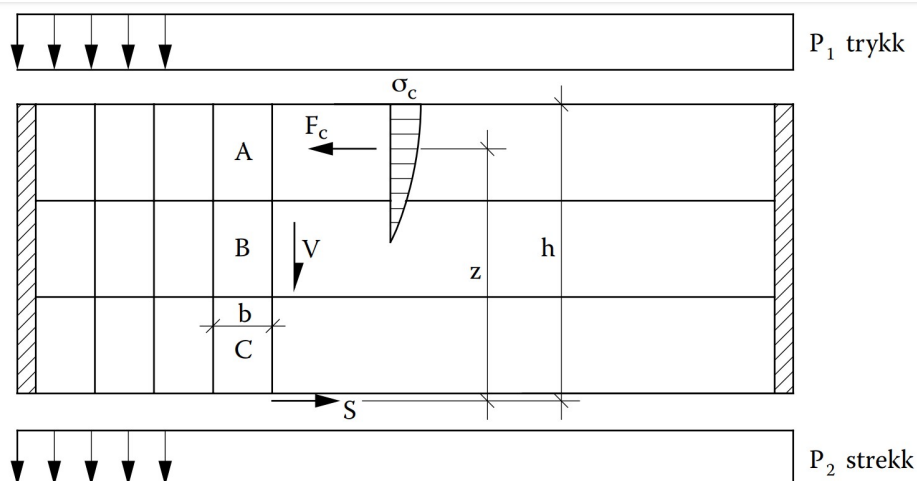
Figure 2.9 has similarities to Figure 2.6, but the elements forming the monolithic floor is divided into zone A, B and C. Figure 2.9 is sourced from BEB Volume B ch. 12.4.4. The free-body diagram of the zones shows how the shear stresses are transferred through the floor. τ_h represents the in-plane shear stresses acting in the horizontal direction of Figure 2.9 and consequently the transverse joint of the element. The opposite counts for τ_v which represents the in-plane shear stress acting in the vertical direction Figure 2.9, which corresponds to the longitudinal joint. Figure 2.9 illustrates how the compression and tension occur in the concrete and transverse reinforcement respectively. The internal moment arm, z , reaches outside of the floor to the outlying transverse reinforcement.

To calculate the shear stresses, it is necessary to utilize the effective joint height, represented as "effektiv fugehøyde" in Figure 2.9, which is denoted by the symbol t in the calculation. The effective joint height is by Norwegian norms calculated by subtracting 30 mm from the height of the slab:

$$t = h - 30mm$$

Finally, the expression for dimensioning shear stress in the longitudinal joint can be determined.

$$\tau_v = \frac{V}{z \cdot t}$$



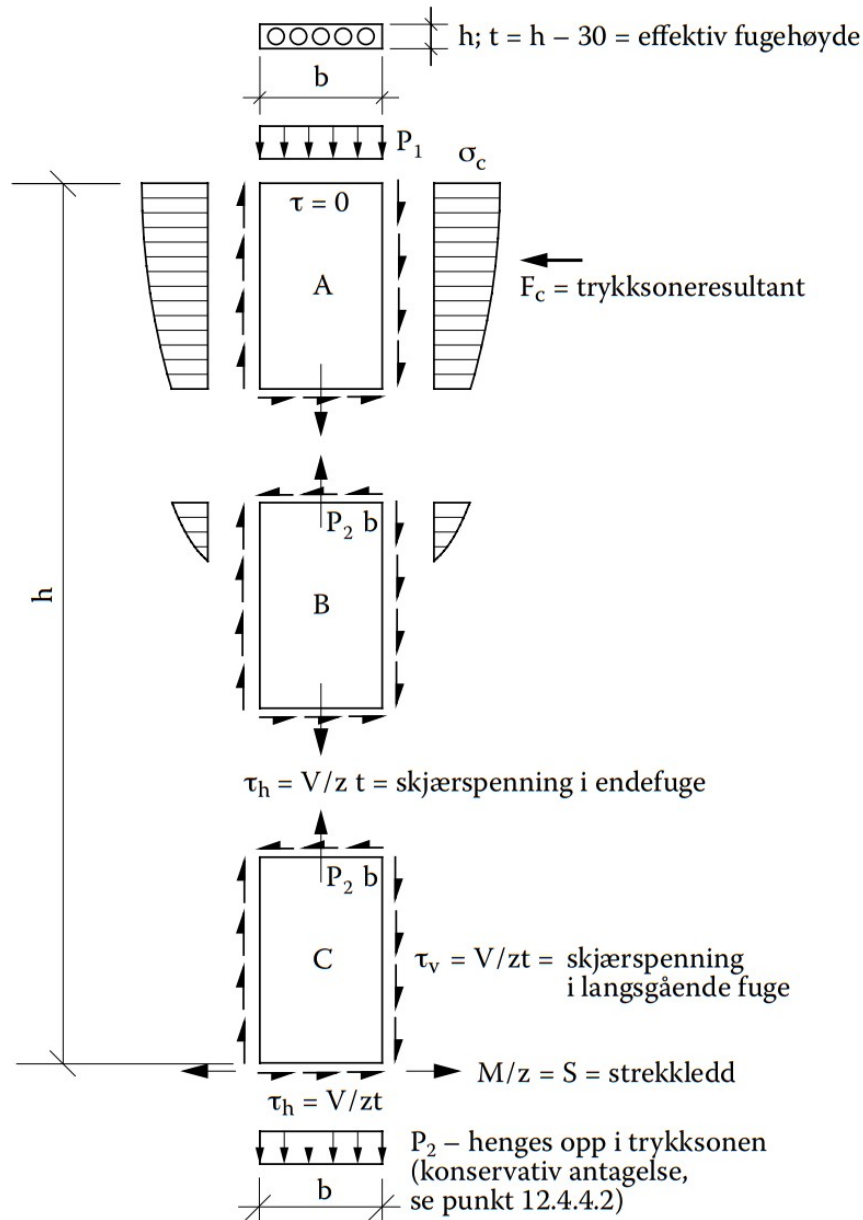


Figure 2.9: Monolithic floor built up by elements thereafter divided into zones [12]

According to EC2 6.5.3 [17], the design value of shear stress at the interface between concrete cast at different times is defined as:

$$v_{Edi} = \beta \frac{V}{z b_i}$$

where β represents the ratio between the longitudinal force in the new concrete area and the total longitudinal force, while b_i is the width of the interface. This approach is not very suitable for HCS because it is mainly intended for topping concrete on decks and beams, in addition to wall joints. Therefore, it is chosen to emphasize the expression for the design value of shear stress provided in BEB.

2.5 Friction

When a normal compressive force is acting on an interface, shear forces may be transferred along an interface due to friction, according to fib 8.3.3 [15]. Figure 2.10 provides a clear visualization of the frictional effect. Birkeland and Birkeland [18] applied this approach to estimate the shear capacity of concrete joints. Although this model seems very simplified for non-regular shaped concrete interfaces, Carlsson [19] showed that aggregate crushing in the first slip phase would lead to uniformly distributed stresses. The most pronounced irregularity would be loaded first, creating big concentrated stresses, leading to the crushing of these tips and edges. Subsequently, a successive degradation would occur as the slip continues, creating a saw-tooth-shaped interface. The degradation depends on the compressive stress, roughness, and strength of the concrete [19].

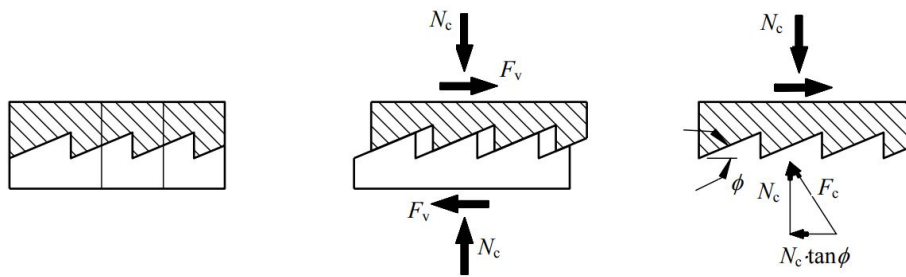


Figure 2.10: Schematic illustration of shear transfer by friction [15]

Equilibrium gives the relation between shear capacity, F_v , and normal force, N_c . The frictional coefficient, μ , which is equal to:

$$\mu = \tan(\phi)$$

gives the relation:

$$F_v = N_c \tan(\phi)$$

Shear capacity and normal force divided by the area of the surface give the shear stress relation:

$$\tau_R = \mu \cdot \sigma_c$$

where the compressive stress, σ_c , is acting normal to the concrete interface.

This approach requires assumptions that need to be fulfilled [18]. Firstly, the reinforcement needs to be sufficiently anchored on both sides of the failure plane. Secondly, it requires that the surfaces are clean, having removed sawdust, loose rust and other polluting materials, as stated by Birkeland and Birkeland [18].

Walraven and Reinhardt [20] had a slightly different way of modelling concrete friction. Concrete can be divided into matrix and aggregates, with greater strength and stiffness for the aggregates. Cracking occurs through the matrix in the bond zone and at the circumference of the aggregate particles, which is the weakest link in the system. Hardened cement paste is a visco-elastic material, which means that deformation by initial sliding is partially elastic and partially plastic. As

illustrated in Figure 2.11, the shaded area represents the matrix parts which has disappeared due to plastic deformations of the matrix. This is due to initial sliding resulting in stress concentrations around the aggregates. Hence, further plastic deformations occur until an equilibrium of forces is obtained. This model is called the "aggregate interlock model". Figure 2.12 also illustrates the contact areas during shear displacement with the shaded area as plastic zones.

The validity of the aggregate interlock theory and its belonging equations has been checked for concrete strengths up to 65 MPa by Walraven and Reinhardt [20]. They point out that cracks in high-strength concrete will be smoother because the matrix strength is so high that aggregates will fracture at the crack formation. The resistance against cracks will therefore not behave according to the interlock model in these cases and instead, a more brittle failure will occur [20]. The surface needs a certain roughness in order to obtain the interlock mechanism. For smooth surfaces, the shear resistance will follow the traditional frictional concept, where the capacity is dependent solely on the frictional coefficient and the compression force at the interface. According to fib 8.3.3, friction between surfaces of the concrete cast at different times is generally classified as a *smooth* interface [15].

Nevertheless, the two models are based on the principle of a separation between the faces when sliding occurs, which creates tension in the reinforcement creating compressive forces on the surfaces. This compressive force makes shear resistance by friction possible and is further described in Section 2.6.

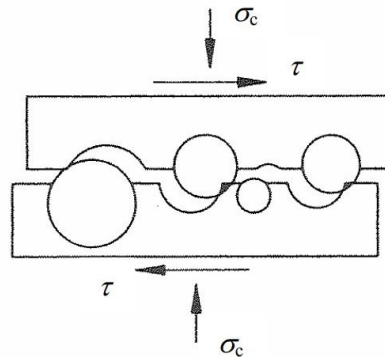


Figure 2.11: Shear transfer by aggregate interlock, according to Walraven and Reinhardt [20]

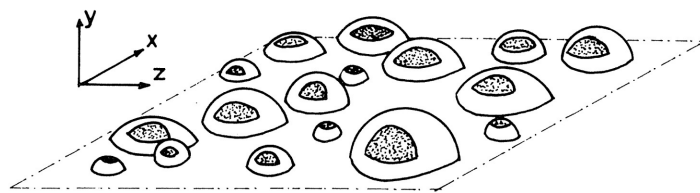


Figure 2.12: Shaded area marks the plastic deformations of the matrix [20]

2.6 Compressive forces due to transverse steel

According to fib 8.3.4, the shear capacity due to friction is dependent on a compressive force acting on the joint [15]. For HCS, this can be solved by the influence of transverse steel. Under shear loading slip, a joint separation will occur due to the irregularities of the concrete interface, as Figure 2.13 shows. This separation will induce tension in the transverse steel reinforcement crossing the joint. Due to equilibrium, this tensile force will create a compression force acting on the joint interface, as Figure 2.13b shows. Therefore, separation of the joint generates compression forces making the shear transfer by friction possible, even without initial compression at the interface [15]. Xia et. al. showed that the shear capacity increases significantly after adding reinforcement, creating compression at the interface. However, the relation did not appear to be linear, meaning that a further increase in the amount of reinforcement only gave a marginally higher shear resistance [21].

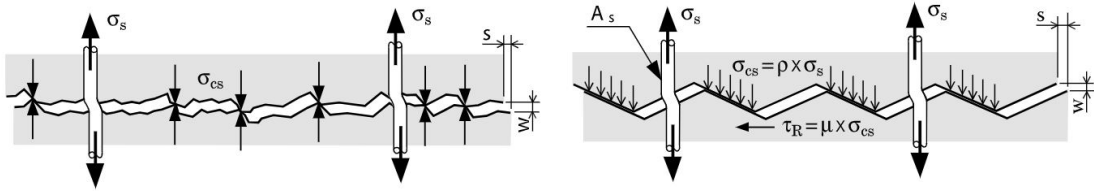


Figure 2.13: Transfer of shear force in grouted joints [12]

Joint separation increases with increasing slip until maximum separation, w_{max} , occurs. From this point, an increased slip will not create a bigger joint separation. When a certain slip has occurred with an adjoining separation, w , the clamped steel bars have got an elongation equal to it. If the transverse bars are not embedded in the concrete, the elongation in the steel can be assumed to be uniformly distributed through the whole length of the bar. This gives a strain, ϵ_s , and stress, σ_s , equal to respectively

$$\epsilon_s = \frac{w}{l_a}$$

$$\sigma_s = \epsilon_s \cdot E_s$$

The total tensile force in the bars generates a compressive force of the same magnitude across the joint. Therefore, the compressive stress could be expressed as,

$$\sigma_{cs} = \frac{A_s}{A_c} \cdot \sigma_s$$

However, the bars would be expected to have some sort of embedment into the concrete. Reinforcement in concrete generally has a good bond and could therefore transfer shear by friction. With a big slip, the bar would be subjected to dowel action, which will increase the shear capacity

of the joint. However, maximum capacity due to dowel action occurs at a bigger slip than for maximum shear friction capacity. Therefore, the maximum shear capacity will not be the sum of the maximum capacity for each contribution.

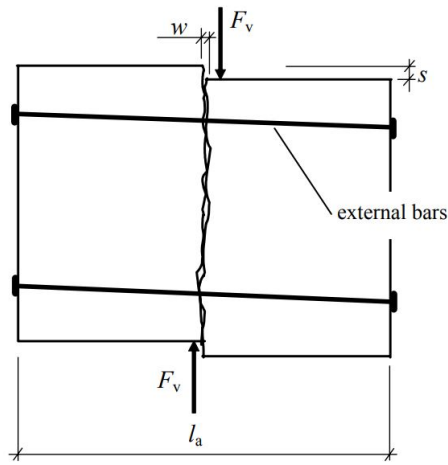


Figure 2.14: External transverse bars not embedded in the concrete [15]

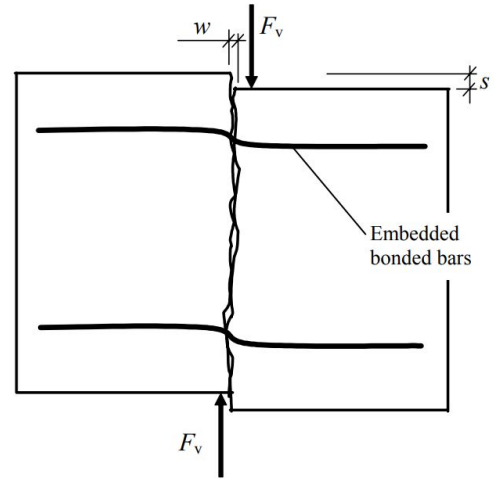


Figure 2.15: External transverse bars embedded in the concrete, anchored by bonds [15]

As stated in EC2 10.9.3(7): "Transverse reinforcement for shear transfer across connections in the diaphragm may be concentrated along supports, forming ties consistent with the structural model. This reinforcement may be placed in the topping, if it exists". Consequently, the standard allows for transverse bars to be put close to the supports, without needing to evenly distribute the reinforcement over the length of the joint.

According to fib 8.4.2.1, the shear capacity was almost proportional to the normal stress applied. However, it was noted that the shear capacity was more dependent on the compressive stress for higher concrete strength in the joint, as Figure 2.16a from fib shows. Additionally, the capacity of the joint is significantly dependent on the joint length for high-strength concrete, as Figure 2.16b shows. This can be explained by high stresses near the end of the joint, resulting in critical stresses in these regions, while the interior parts experience lower stress. The lack of redistribution of stresses for high-strength concrete leads to a more brittle behaviour, as stated in fib 8.4.2.1 [15].

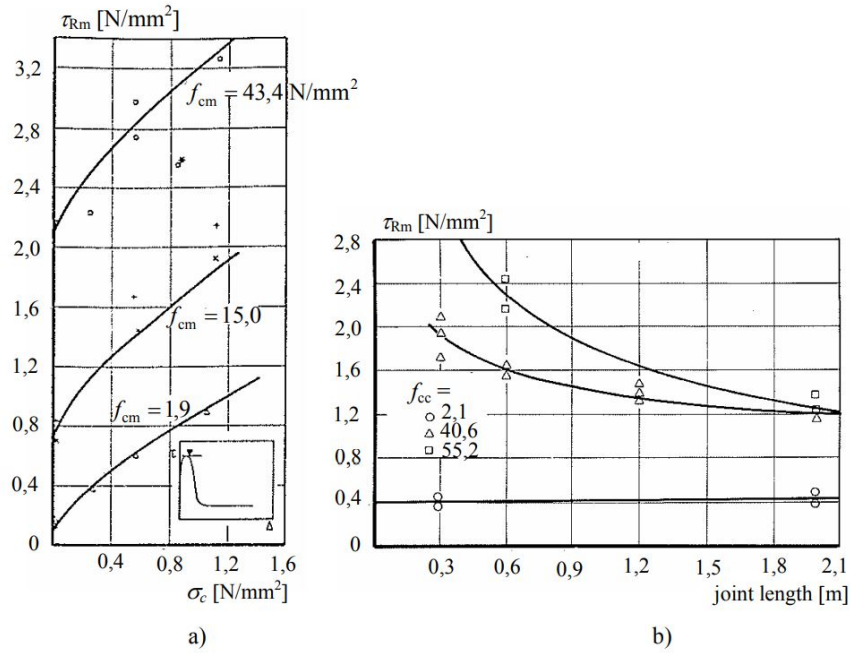


Figure 2.16: Shear strengths of joints with varying joint strength [15]

2.7 Design shear capacity in connections with concrete-to-concrete interfaces

The EC2 6.2.5 [17] provides a general expression to determine the design shear resistance of concrete interfaces cast at different times, which can be utilized as an equivalent expression to determine the design shear resistance between HCS and neighbouring grouted joint, as stated in fib 8.4.3 [15]. The design shear resistance of the longitudinal connection between HCS depends on the adhesion bond and friction between the two concrete interfaces [22]. The external normal force acting across the interface causing the friction can either arise from the transverse rebars, as described in 2.6, or from direct external forces. It is vital to ensure that the design shear resistance stress, v_{Rdi} , is lower than the concrete's upper limit for compression capacity to prevent local crushing. This upper limit is determined in EC2 6.2.2(6) [17] and further described in Section 2.8. EC2 6.2.5 provides the following expression to calculate the design shear capacity.

$$v_{Rdi} = c f_{ctd} + \mu \sigma_n + \rho \sigma_n (\mu \sin(\alpha) + \cos(\alpha)) \leq 0.5 \nu f_{cd} \quad (2.1)$$

The first expressions of equation 2.1, $c f_{ctd}$, represents the contribution from the adhesion bond strength where c is the adhesion bond coefficient and f_{ctd} is the concrete tensile design strength. According to fib 8.5.1.1 [15], cracking along the joint interface cannot be avoided due to temperature fluctuations and shrinkage effects. The cracks will occur at the interface due to precast units having a very large in-plane stiffness compared to the joints [15]. Therefore, in calculations for joint capacity, the joint is assumed cracked. According to fib 8.1, when a joint is cracked, the contribution

of the adhesion bond to shear transfer becomes negligible and is thus neglected [15]. In addition, the adhesion bond depends largely on workmanship factors performed on the construction site. The conditions of the joint surface pre-casting are essential for the adhesion bond. For instance, elements with dirt, sand, or oil on the joint surface can affect the adhesion bond. This increases the risk of conducting calculations with shear transfer from adhesion bond and is therefore advised in fib 8.1[15] to be neglected in the calculations.

Secondly, $\mu \sigma_n$ represents the friction resistance in the joint where μ is the friction coefficient and σ_n is the normal stress per area unit. Normal stress comes from external compressive forces and is often neglected as well. The last part $\rho \sigma_n (\mu \sin(\alpha) + \cos(\alpha))$ represents the capacity component resulting from the presence of transverse reinforcement crossing the interface. The reinforcement ratio is represented by ρ , and α refers to the angle between the joint and shear reinforcement. In the case of joints between HCS, the shear reinforcement is laid perpendicular to the joint ($\alpha = 90^\circ$). Inserting α equal to 90 degrees gives the expression relevant for HCS:

$$v_{Rdi} = \rho \sigma_n \mu \leq 0.5 \nu f_{cd} \quad (2.2)$$

Furthermore, equation 2.1 can be multiplied with the concrete joint interface area, A_c , to get the design shear force, V_{Rd} :

$$V_{Rd} = c f_{ctd} \cdot A_c + \mu N_{Ed} + \rho \sigma_n (\mu \sin(\alpha) + \cos(\alpha)) \cdot A_c \leq 0.5 \nu f_{cd} \cdot A_c \quad (2.3)$$

Assumed transverse shear reinforcement perpendicular to the joint and full yielding in the reinforcement, the expression for design shear force is:

$$V_{Rd} = c f_{ctd} \cdot A_c + \mu N_{Ed} + \rho f_{yd} \mu \cdot A_c \leq 0.5 \nu f_{cd} \cdot A_c \quad (2.4)$$

According to EC2 6.2.5, concrete surfaces can be divided into four categories as listed in the bullet points below with associated coefficients for the adhesion bond and friction in Table 2.1 [17]. HCS surface falls under the category "Smooth" with corresponding adhesion factor, c , equal to 0.2 and friction factor, μ , equal to 0.6

- Very smooth: A surface cast against steel, plastic, or specially prepared wooden molds.
- Smooth: A slip formed or extruded surface, or a free surface left without further treatment after vibration.
- Rough: A surface with at least 3 mm roughness at about 40 mm spacing, achieved by raking, exposing aggregate or other methods giving an equivalent behaviour.
- Indented: A surface complying with the requirements illustrated in Figure 2.17.

Table 2.1: Adhesion bond and friction values for different surface classifications

Separating action		
Classification	Adhesion bond c	Friction μ
Very smooth	0.025-0.1	0.5
Smooth	0.2	0.6
Rough	0.4	0.7
Indented	0.5	0.9

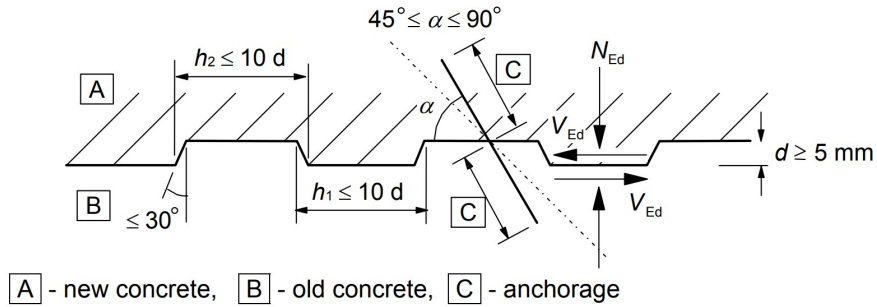


Figure 2.17: Requirements in order to classify the surface as indented [15]

In joint connections where there is assumed to be no adhesion, the normal stress acting perpendicular to the joint can be assumed as:

$$\sigma_n = v_{Rdi} \cdot \mu \quad (2.5)$$

According to Gustavsson, shear transfer of joints is not influenced only by its irregularities [23]. Factors such as workmanship, joint cleanness, compaction, curing, and concrete wetting, all of which he emphasizes have at least the same importance. Furthermore, an experienced assembly manager of precast elements at Spenncon AS, Bjørn Ove Mork, has been interviewed regarding the development of the casting process of joints in recent years [24]. Mork emphasizes that the quality of joint work has improved significantly in the last 40 years. Mork further explains that during the 1980s, the joint concrete was drier and distributed manually using a wheelbarrow. Additionally, when the joint concrete became too dry during casting, more water was simply added to the concrete on-site. As a result of this, Mork describes today's process as much more controlled by standard procedures and measurements than before. He clearly emphasizes that the execution process and joint concrete have a significantly higher quality [24].

According to EC2 10.9.3(12) [17], the average longitudinal shear capacity, v_{Rdi} , should not exceed 0.1 MPa for 'very smooth' surfaces and 0.15 MPa for 'smooth' and 'rough' surfaces. Notably, this shear capacity refers to the average shear stresses along the joint. This means that the joint can withstand higher stresses for local sections along the longitudinal joint. It appears

that the requirement for average longitudinal shear capacity from EC2 lacks a logical explanation and supporting arguments, and its origin cannot be determined. Nonetheless, this simplification makes calculating shear capacity easier. On the other hand, BEB volume C 13.1.2.1, argues that disregarding the compressive strength in the joint when determining the upper limit for shear capacity is too conservative [12]. Therefore, BEB table C 13.2 offers an alternative average longitudinal shear capacity for HCS. *Smooth* surfaces are presented to have an average shear capacity equal to 0.188 MPa for B30 concrete and 0.208 MPa for B35 concrete. The latter capacity is based on 20% of the design tensile strength, f_{ctd} .

However, in the upcoming revised version of EC2 the limit for average shear stress in longitudinal joints is removed [25]. For instance, this implies that the average longitudinal shear stress can exceed 0.15 MPa for *smooth* surfaces. The upcoming revised EC2 13.6.2(4) states; "diaphragm actions provided by untopped building floors made of precast slab elements with concrete or grouted longitudinal joints, their shear resistance should be determined according to shear-friction mechanisms, accounting for the transverse compressive force on the joint surface and for its roughness or presence of keys". This implies that the contribution from adhesion to the shear capacity is neglected in future calculations when there is no topping layer contributing to diaphragm actions. As mentioned earlier in this section, it is a common practice to frequently disregard the contribution from adhesion due to cracked joints caused by temperature fluctuations and shrinkage. The exception is joints close to stairwells, where the adhesional effects can be included in the calculation.

2.8 Upper limit for the shear capacity

According to equation 2.4 for the shear capacity of concrete cast at different times, the shear capacity of joints increases with an increased amount of transverse reinforcement. However, the concrete has an upper limit regarding compressive capacity. Local crushing of the concrete will occur if the compressive forces exceed the concrete compressive capacity. Hence, there is an upper limit for the amount of transverse steel that can be used in a joint [15].

Equilibrium gives the correlation between compression forces and the shear force. The crack propagates 45° from the tensioned reinforcement. Hence, the shear force could be expressed as

$$V = 0.5 \cdot \sigma_c \cdot b \cdot z \quad (2.6)$$

These mechanics are used to determine an upper limit for shear compression capacity in standards. According to EC2 6.2.5(1) p. 90 [17], the upper limit for the shear capacity is given by

$$v_{Rdi, max} = 0.5 \nu f_{cd} \quad (2.7)$$

where ν is determined as,

$$\nu = 0.6 \left[1 - \frac{f_{ck}}{250} \right] \quad (2.8)$$

ν is the capacity reduction for cracked concrete due to shear forces.

The combination of tensile forces in the reinforcement and shear forces along the joint interface results in an inclined compressive resultant across the interface. The series of inclined compression forces are held in equilibrium by transverse steel bars [15]. The biaxial state of stresses reduces the compressive strength and is limited by νf_{cc} , which is the compressive strength of concrete subjected to uniaxial stress.

2.9 Joint assembly

BEB volume G ch. 4.1.5 and 7.5.2 provides guidelines and instructions for assembling HCS with joint connections [12].

The joints in prefabricated building elements often need to transfer large forces, and in addition, the material must protect the joint reinforcement against corrosion and ensure that the construction is watertight. Before the concrete is poured, the joint should be cleaned and watered. All loose particles such as dust, concrete residue, snow, ice, etc. need to be cleaned using compressed air, a steamer, a broom, or similar. During winter, a steamer should not be used as the condensation can freeze [24]. Under normal conditions, a flowing, fine-grained concrete of at least B30 is used. Formworks need to be mounted with plates where the joint is abnormally wide, and insulation foam, or similar, can be used elsewhere.

The concrete can be either delivered from a concrete factory or mixed on-site. The concrete can be poured in various ways, but it is most common to spread it using a wheelbarrow or pump it directly from the concrete truck. When the joint is grouted with concrete, the top surface of the deck can be cleaned using a squeegee, and the bottom surface by using a broom. When subjected to high air temperatures, generally over 20°C, the deck should be watered after 2-3 hours, according to Mork [24].

When constructing in the winter months, it is important to consider the temperature when selecting the cement paste. It is essential to use frost-free cement because the joint usually demands small volumes, so the heat of hydration is not enough to prevent freezing of the fresh concrete. Other actions to avoid frost damage are to use heated mortar, rapid-setting cement, additives, and external heat. In addition, when casting in sub-zero temperatures, it becomes necessary to heat the HCS before casting. The HCS is covered with tarpaulin to facilitate this, while a heat pump is positioned inside to increase the temperature. As a result, the HCS has a temperature over zero degrees before casting, preventing the hardening rate from decreasing [24].

3 Previous studies

3.1 Walraven and Reinhardt 1981

A publication by Walraven and Reinhardt from Delft University presents theory and experiments on the mechanical behaviour of cracks in plane, and reinforced concrete subjected to shear [20]. The tests conduct shear displacement tests on concrete specimens with different crack widths. The publication discusses the theory of aggregate interlock, which was previously introduced in Section 2.5.

One of the conducted experiments involved applying a crack to the specimens, initiating shear displacement, and using external restraint bars. The test setup is illustrated in Figure 3.1. The results show that increasing concrete quality results in increased shear and normal stress capacity. Furthermore, the test showed that if the shear stress were increased and the normal stress remained unchanged, it would lead to failure due to slip. On the other hand, if the normal stress surpasses a specific combination of shear displacement, shear stress and crack width, no significant effect would occur.

One of the conclusions from the publication was: "Shear transfer across cracks cannot be simply formulated as a relation between shear stress and shear displacement, but in a more complex mechanism, in which shear stress, shear displacement, normal stress and crack width are involved".

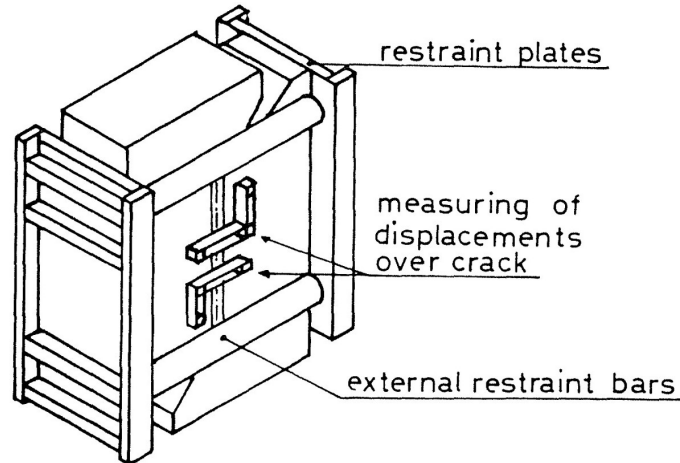


Figure 3.1: Test setup of specimens with external restraint bars [26]

3.2 Composite concrete-to-concrete bond

The friction and adhesion coefficients are central in determining the shear capacity between concrete cast at different times. Mohamad et al. [26] performed a "push-off" test with five different surface roughnesses and varying normal stresses to compare friction and adhesion values with standard values from EC2. In this test, fresh concrete is cast to an already hardened concrete and cured

before testing. The old concrete is fixed to the setup, and a horizontal force pushes the new top layer until failure. This test method is similar to the one described in Section 5.2, and is illustrated in Figure 3.2.

The results from the push-off test are presented as plots in Figure 3.3, where the solid line represents the specimens with *smooth* interface. Observing the shape of the shear force function and how it changes when the normal stress is increased is significant. Firstly, the shape is similar for all normal forces, with a substantial slip followed by a friction phase. Plot (b), with 0.5 MPa normal stress, deviates from the other plots. If plot (b) is neglected, it is observed that the slip occurs at approximately the same force for all plots, but for the friction phase, the load increases when the normal stress increases.

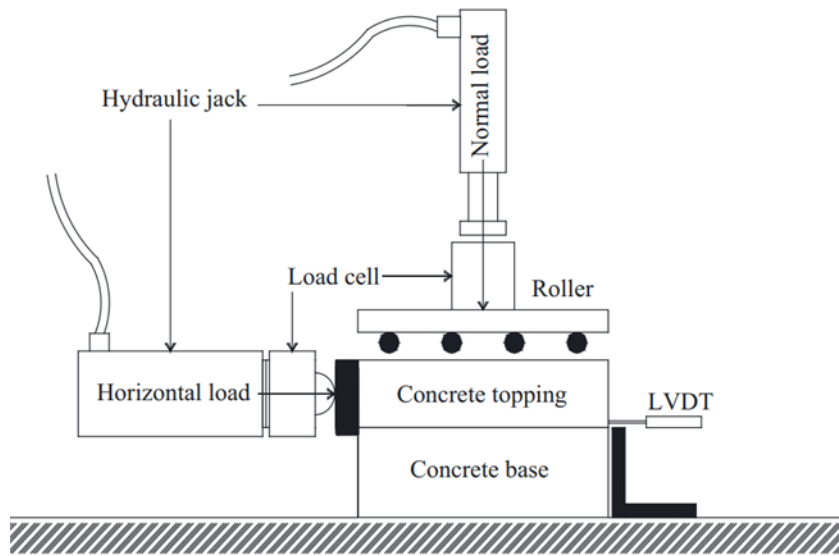
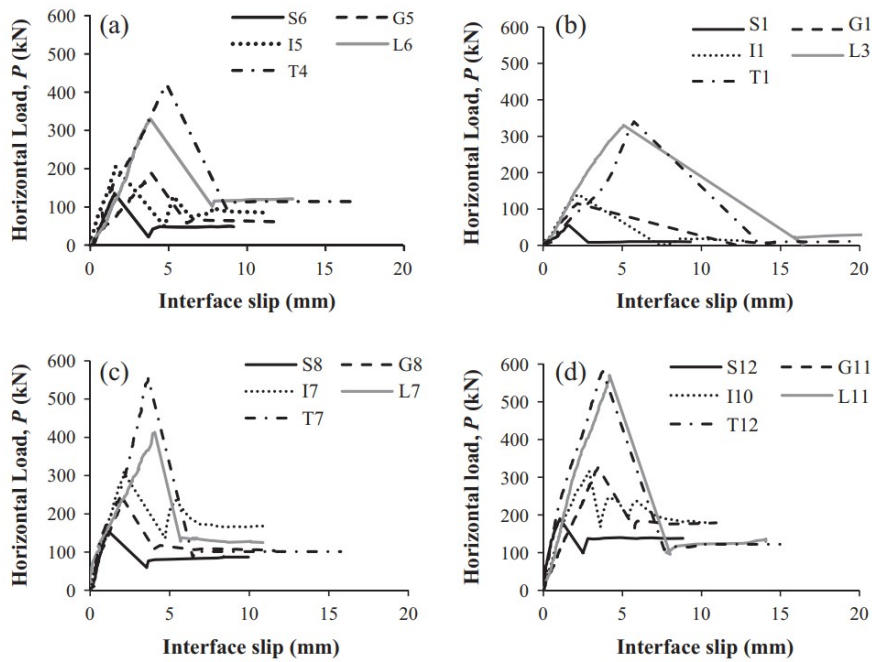


Figure 3.2: Test setup[26]



$S = \text{Smooth}, G = \text{Groove}, I = \text{Indented}, L = \text{Longitudinal Roughened}, T = \text{Transverse Roughened}$

Horizontal load–interface slip relationship for (a) $\sigma_n = 0 \text{ N/mm}^2$, (b) $\sigma_n = 0.5 \text{ N/mm}^2$, (c) $\sigma_n = 1.0 \text{ N/mm}^2$, and (d) $\sigma_n = 1.5 \text{ N/mm}^2$.

Figure 3.3: Results obtained from the application of different surface roughnesses under varying normal stress levels[26].

The publication concludes that the friction- and adhesion coefficients increase as the degree of roughness increases. When the surface roughness is enhanced, it provides a larger contact area for the concrete adhesion bond and thereby increases the adhesion coefficient. Meanwhile, the friction coefficient increases with the degree of roughness.

The test results showed both a higher friction- and adhesion coefficient for surface type classed as *smooth* compared to standard values from EC2. The frictional coefficient shown in the experiment is equal to 0.84 (0.60 in EC2) while the adhesion coefficient is equal to 0.27 (0.20 in EC2).

According to Mohamad et. al [26], shear capacity equations are based on a static friction condition, which applies to the aggregate interlocking stage. The study presents an empirically determined friction coefficient, dependent on the mean peak height of the roughness, R_{pm} , of the surface. The study showed that the relation between friction and roughness is non-linear and the incline diminishes for increased roughness, as illustrated in Figure 3.4a. This indicates that a small increase in roughness leads to a significantly higher friction coefficient for *smooth* surfaces. In contrast, the adhesion has a non-linear relation to the roughness but with an increasing relation for increased roughness, as shown in Figure 3.4b.

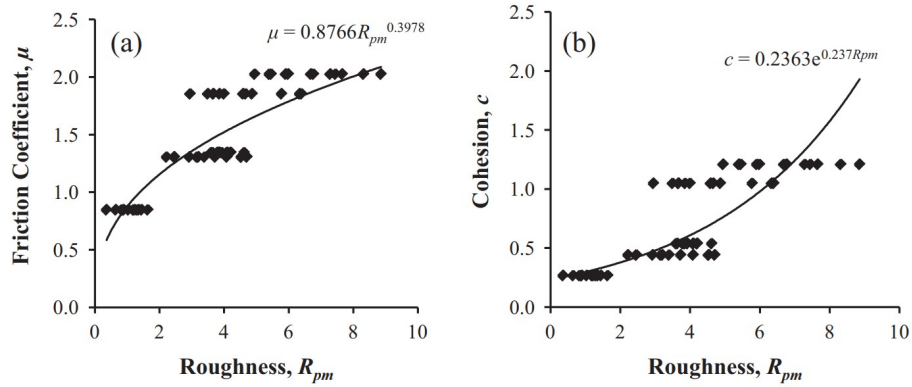


Figure 3.4: Relationship between friction coefficient and roughness parameter. Adhesion is referred to as cohesion [26]

3.3 Various research applications with potential relevance

It is valuable to study shear tests conducted with other materials to gain a comprehensive understanding of shear transfer. Studies of shear mechanisms for pullout of rebars could be relevant to get insight into shear-related issues and is a subject area with more research conducted compared to shear transfer in concrete-to-concrete interfaces. According to fib 7.2.2, the relationship between shear stress and slip will follow the graphs shown in Figure 3.5a for rebars pulled out of concrete. Figure 3.5b further illustrates the distinct phases during a pullout. At low levels of slip, the dominant contribution stems from adhesion, while the shear key resistance dominates the capacity in the following phase. The maximum capacity is reached just before the shear keys are crushed. After the crushing of shear keys, the capacity drops before reaching the frictional phase, where the capacity is solely dependent on friction. Although this study focuses on shear transfer between concrete and steel, it offers opportunities for comparisons to shear stress mechanisms for concrete-to-concrete interaction. The shear keys on rebars are much greater than the possible shear keys formed by aggregates on concrete surfaces, but it could be valuable to study its similar behaviour.

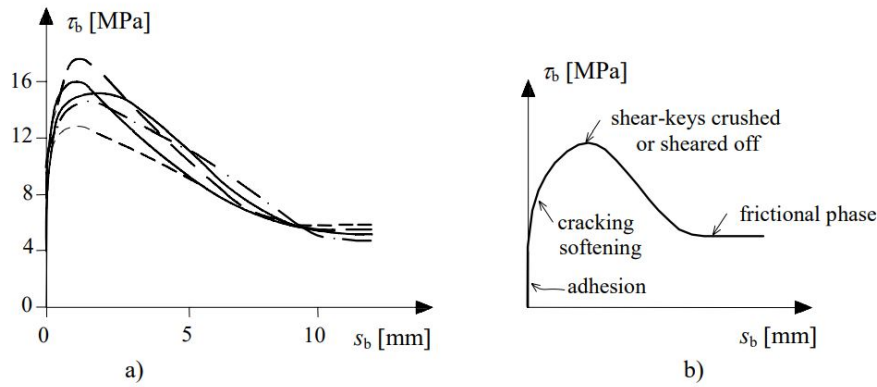


Figure 3.5: Relationship between bond stress and slip for rebar pullout [15]

The ACI Structural Journal published a study examining bond stress-slip prediction under pullout of a rebar [27]. This publication addresses research similar to the content presented in fib 7.2.2 [15]. Still, it provides a more detailed explanation of the transition from shear-key failure to the frictional phase. As illustrated in Figure 3.6, the turning point labeled "Shear-off of concrete keys" signifies the transition to the frictional phase, where a substantial amount of concrete keys are shredded off. Furthermore, this transition potentially indicates the shift between the friction theories of aggregate interlock proposed by Walraven and Reinhardt and the "saw-tooth-shaped interface" theory proposed by Birkeland and Birkeland and supported by Carlsson [20][18][19]. These theories are previously described in Section 2.5 and will be further discussed in Chapter 7.

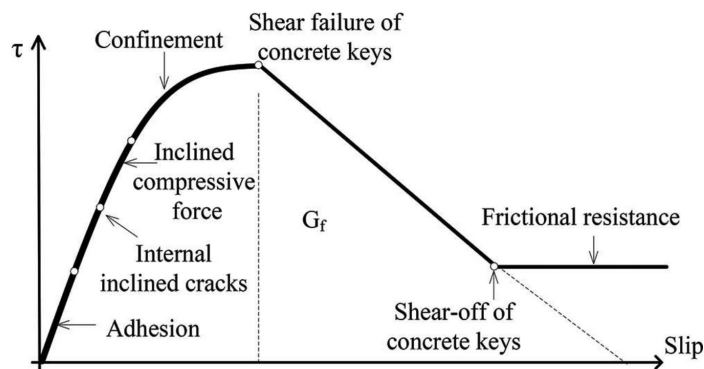


Figure 3.6: Relationship between bond stress and slip for rebar pullout [27]

Furthermore, fib 8.4.1.1 provides insights into the shear-slip relationship observed in connections between wall panels [15]. The capacity of connections with shear keys relies on the concrete failure of these shear keys. At the peak of shear stress, local cracking or crushing occurs. After the drop in shear stress, the shear transfer is mainly carried out by shear friction in the residual stage. On the other hand, connections without shear keys rely solely on shear friction, resulting in approximately constant shear stress. The effect of shear keys is schematically illustrated in Figure 3.7.

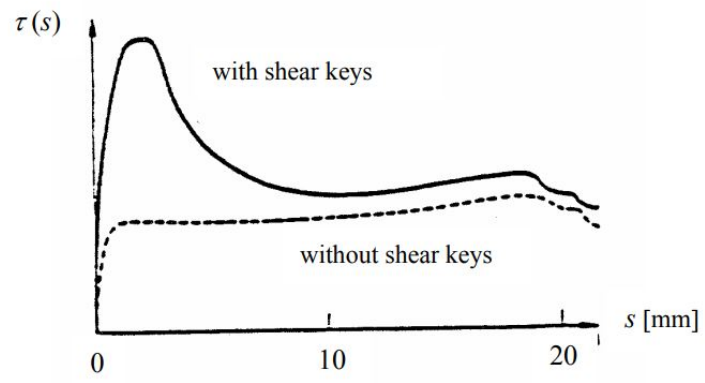


Figure 3.7: Typical shear-slip response of joints with and without shear keys [15]

4 Disassembly process of HCS today

In Norway, only a few companies have experience reusing HCS. Among these companies, Øst-Riv AS stands out for their involvement in projects such as the KA13 reuse project [1][28]. To gain further insight into the disassembling process, the authors of this thesis visited one of their sites located at Lysaker, Oslo. At the Lysaker site, there was an ongoing disassembly of a building from the 1980s with the intention of reusing its concrete elements in the construction of a new building at the same location. This reuse of concrete elements is essential to achieve the "Outstanding" classification in BREEAM-NOR [9]. Based on the visit to Lysaker and the experience report from the KA13 project, the following section will describe the disassembly process of HCS used today and the accompanying relevant topics.

4.1 The disassembly process

To begin the disassembly process, all non-structural components must be removed until only the fundamental building structure remains. A tower crane must be installed on-site to lift the HCS off the building and onto trucks transporting them to a large storage hall. Here, the elements are stored and certificated before reuse.

The first on-site step is to mount builder trestles under the HCS, as illustrated in Figure 4.1. When the HCS are released from the supports, these trestles prevent the HCS from falling down.



Figure 4.1: Builders trestles placed in the floor below the relevant HCS

Secondly, a large concrete saw mounted on rails cuts the short edge of the HCS on the inside of the transverse supports. The saw is shown in Figure 4.2, and it is noticeable how a portion of

the HCS remains attached to the support beam after cutting. This offset is to avoid the complex removal of the connection between the HCS and support beam, as this connection involves both vertical and horizontal steel dowels, which are grouted together at the end joint.

Therefore, cutting a distance from the edge reduces complexity and results in a more uniform HCS, but at the expense of a shorter span length. Additionally, this saw is challenging to use, as it requires a significant amount of time to mount and has low accuracy, despite being mounted on a rail system.



Figure 4.2: Concrete saw on rails cutting the short edge

Once the transverse supports are cut off, the HCS is only connected to the structure by the longitudinal joints. The disassembly process of the HCS begins with the outermost element, followed by the removal of each subsequent element inwards. This results in only one longitudinal joint connecting the outermost element. Due to the reduced support, it is therefore common that the HCS detaches and falls onto the builder trestles when the HCS are cut from the transverse supports. In Figure 4.3, the HCS has not detached, and the construction worker measures the distance to the grouted joint before using a jackhammer to remove the grouted joint. Eventually, the joint will open, and the remaining joint bonded to the HCS must be removed, as illustrated in Figure 4.4.



Figure 4.3: Closed joint. Measurement to locate the grouted joint



Figure 4.4: Open joint. Removal of residual joint with the use of a jackhammer

To facilitate the removal of the grouted joint when the adhesion is strong, the crucial step is to achieve separation between the joint and the HCS. Achieving separation will result in the joint being cantilever and less redundant against blows from the jackhammer. If separation is hard to accomplish, a specialised tool commonly used in the rock industry can be utilized. An illustration of this three-pieced wedge can be seen in Figure 4.5 and 4.6. The jackhammer is used to crush a hole in the grouted joint, so the tip of the wedge can be inserted. The plug in the centre of the wedge is then repeatedly hammered until separation is achieved over the entire length of the joint.



Figure 4.5: Wedge



Figure 4.6: Three-part wedge tip

It is necessary to have an open grouted joint to detach and make it possible to put lifting straps around the HCS. Figure 4.7 shows the lifting procedure from the visit at Lysaker, where the straps were encircled around the cross-section of the HCS. On the other hand, Figure 4.8 illustrates the

solution from KA13 where the grouted joint was impossible to remove. This made it challenging to get sufficient space to encircle the lifting straps. Consequently, a new solution was developed, as illustrated in Figure 4.8. This solution is more time-consuming compared to the solution used at Lysaker, as it requires holes to be drilled for the supporting UPE140 beams. Additionally, the drilled holes need to be filled with concrete, resulting in increased costs.

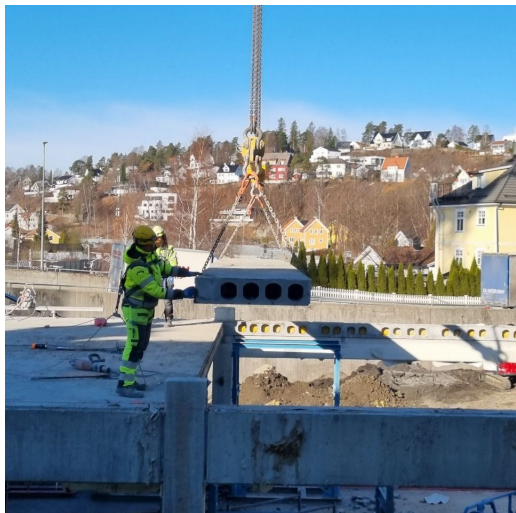


Figure 4.7: Solution from Lysaker. Lifting straps encircled around the cross-section of the HCS

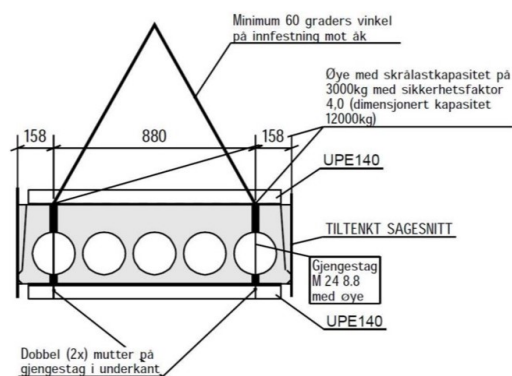


Figure 4.8: Solution from KA13. Lifting straps mounted through drilled holes and with supporting steel beams

Now, the HCS are lifted off the building and onto a truck which is transporting them to a storage facility. Usually, they are stored at a producer of HCS, who has the necessary equipment to verify the HCS for further use. The HCS are cleaned, tested and verified before they are reused in new buildings. In 2022, a new Norwegian standard was introduced, NS 3682:2022 *Hollow core slabs for reuse* [29]. This standard provides requirements and guidelines for the planning, dismantling, processing, testing, assessment and documentation of used hollow core slabs for reuse. While there are existing standards for production control of newly produced HCS with requirements for CE marking, these standards do not meet the possibility to assess already produced HCS. NS 3682 adds the possibility of assessment and classification of HCS for reuse.

4.2 Topics regarding today's disassembly process

Project manager T. Lindseth at the Lysaker project highlighted challenges that must be addressed for disassembly to become common practice [1]. Currently, the production of HCS has a relatively low cost compared to expenses related to reusing elements. Given the time gap that often exists between disassembly and reuse in new projects, large storage halls are required to store the HCS temporarily. Here, the elements are tested for durability and capacity. There could be months of storage before the elements are reused in new buildings, increasing the process cost [1]. In the KA13

reuse project, it was also experienced issues regarding the lack of reused second-hand materials at the market due to few complex disassembly projects [28]. They also experienced an increased need for cooperation with the planning engineers, since the blueprints were updated continuously as few suitable construction elements were found at the second-hand market.

Lindseth emphasized the potential for reuse of HCS in situations where complex demolition is required. For instance, during Øst-Riv's remodelling of hotel The Hub, Oslo, the building site was very cramped for space, and the entire HCS had to be lifted out to deal with logistics [28]. In contrast, a hypothetical scenario of a building in the middle of a field does not require specific demolition methods and will be wrecked down using conventional methods, according to Lindseth. For these scenarios, demolition will always be more economical and less time-consuming due to a huge gap in time and cost of current procedures. He emphasizes that governmental intervention through taxation and subsidies is essential for a full-scale industry change. As a result, requirements and laws related to reuse will develop the construction industry towards more efficient methods. Finally, he suggests implementing reuse into the design process more frequently will contribute to improving the process [1].

Deconstruction versus demolition of existing structures has been studied to some extent. The master's thesis of Van den Brink discusses the factors affecting the possibility of reusing concrete elements and concludes that demolition time in an Amsterdam project is expected to be 2.5 times larger for a reuse project compared to traditional demolition [30]. He discussed that time-consuming factors such as complex cutting and lifting regarding the reuse of the elements occur. However, it is pointed out that if disassembling buildings becomes common practice, both time and cost factors could be reduced significantly [30].

Both Lindseth and van den Brink emphasize the durability of HCS elements as a significant advantage for reuse [1][30]. The majority of HCS elements are located in dry and tempered conditions during their lifespan, reducing the effect of corrosion and creep [30]. According to Lindseth, the durability of HCS increases the value of reuse, as the elements have a much longer lifespan than the building itself. However, the disassembly process poses a risk of damaging the elements. The sawing and lifting process involves the risk of damaging elements, but experienced workers at the construction site can minimize this risk. Lindseth estimates that more than 95 % of the elements are approved for reuse after disassembly [1].

The thickness of the concrete topping needs to be assessed, as it may need to be removed before the cutting process can begin. During the KA13 project, the adhesion between the HCS and the concrete topping was experienced to be very strong. Removal of the topping layer was considered to be too time-consuming. Therefore, it was decided to allow the HCS to be reused with the topping layer [28]. This increased the self-weight of the HCS and created design capacity problems at the KA13 project. This was one of the primary challenges encountered during the project. Since KA13 was planned installed on old piles in the ground, the additional weight was not accounted

for, resulting in restricted, and less use of reused HCS. In contrast, the Lysaker project did not encounter issues with the topping concrete.

Demolishing workers at Øst-Riv report variable levels of adhesion between projects [1]. In the Lysaker project, demolition workers found the disassembly process to be simple and effective due to low adhesion between the HCS and the joint concrete in the longitudinal joints. However, demolition workers have explained that this is not always the case. In certain instances, some elements have required wedging and chiselling of the joint concrete to disassemble and clean the elements. For elements with strong adhesion, demolition workers expect to use up to 2 hours on the same element, compared to around 15 minutes on elements with low adhesion.

In addition, Lindseth emphasizes the span length as an influencing factor on the difficulty of disassembly [1]. A longer span demands a higher thickness of the HCS, increasing the contact surface between the HCS and the joint.

The difficulty of removing the joint cannot be determined before the disassembly process has started. This results in a significant risk regarding economic and progressive aspects for the companies responsible for the projects, as highlighted in Sirk Bygg's annual report [31]. Consequently, this makes the calculation process difficult for both the entrepreneur and the company in charge of the disassembly process.

5 Methodology

Based on the intention of this master's thesis to simplify the reuse of HCS in future buildings through DfD, the current disassembly processes were central to the experiments. The first experiment closely simulated the disassembly processes and provided results valuable for the second experiment. In the second experiment, shear tests were conducted to determine the concrete-to-concrete shear capacity. Both experiments were conducted in the Laboratory for Material Technology at NTNU Trondheim.

5.1 First laboratory experiment; shear stress transfer Separating actions

The first part of the experiment conducted in the laboratory has the following hypothesis:

To what extent does the implementation of separating actions between hollow core slabs and their associated longitudinal grouted joints impact the adhesion bond in practical dismantling processes?

This laboratory experiment intends to acquire data and knowledge regarding the selected separating actions with promising characteristics from the project thesis [13]. The data collected will include the grading of the adhesion between the grouted joint and HCS. Furthermore, knowledge will be gained through visual observation of the physical outcomes. There are multiple ways to investigate adhesion bonding, but in this experiment, the test method is primarily based on the practical disassembly process currently being used.

To explore solutions for reducing the adhesion between concrete cast at different times, various suppliers of formwork oils, as well as concrete technologists, were consulted. As part of the study, both a dry joint and a pre-watered joint were tested to establish reference values for shear capacity. The effect of watering the joint was tested. The Swedish Betonghandboken section 11.6.1 table 2 states that watering of the joint has a positive effect on the adhesion [32]. In contrast, a cling film was tested to establish a reference value for minimal adhesion. Table 5.1 shows the chosen separating actions.

Table 5.1: Separating actions with descriptions

Separating action	
Name	Description
MasterFinish RL 224	Formwork oil
MasterFinish FW 324	Formwork wax
Water	Plain water
Dry (No separating action)	-
Plastic	Cling film
Olive oil	100% refined olive oil
Mapeform MB 700	Formwork oil
Mapeform W 100	Formwork oil
Mapecure 1	Curing membrane
Mapeform Eco Oil 700	Formwork oil

5.1.1 Test components and material properties

To identify the joint's attributes regarding the shear transfer, two HCS cut-offs were placed against each other, simulating a small-scale version of a concrete flooring joint. As Figure 5.1 show, the HCS had a height of 320 mm and a width of approximately 300 mm. 20 HCS cut-offs were paired to create 10 joints with different separating actions. Vertical plywood sheets were mounted on the end of each joint to create a sufficient formwork, as Figure 5.2 shows. Subsequently, the joints were cast in the NTNU laboratorium.

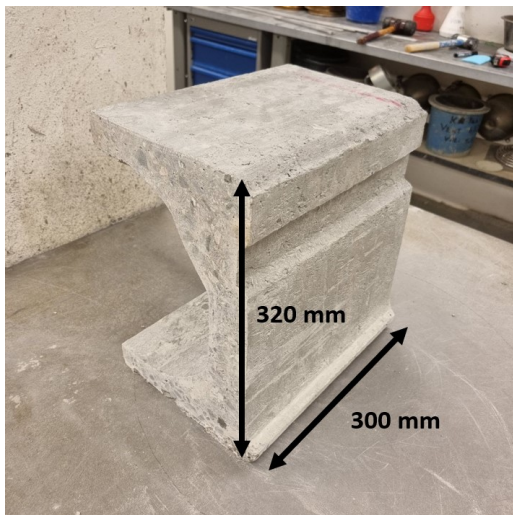


Figure 5.1: Cut off-HCS with measurements

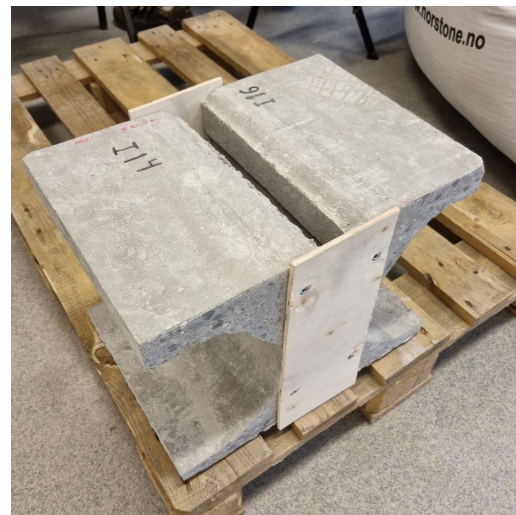


Figure 5.2: Formwork before casting

Joint concrete generally has high workability and a small aggregate size. Therefore, Årdal 0-8 mm aggregate was used, which demanded a very high matrix volume. The concrete proportions had to be adjusted several times to produce concrete with suitable material properties.

Due to their varied characteristics, the separating actions were applied on the concrete surface in different ways. The formwork oils were convenient to apply to the surface with a pressure spray. The spray evenly distributed the oil onto the surface, leaving no dry spots. However, the Mapeform MB700 is a toxic agent containing poisonous aerosols. Therefore, it was unsuitable for spraying and was applied with a small paint brush to prevent the spread of toxic aerosols. The curing membrane Mapecure 1 had a fluidity similar to the formwork oils and was therefore applied with a low-pressure spray. The plastic cling film was applied to the surface with slight slack, allowing it to fill any imperfections during casting. The MasterFinish FW324 formwork wax was tenacious and, therefore, unsuitable to apply with a pressure spray. Consequently, a paintbrush was used to apply it. All separating actions, except the Mapeform MB700, were applied at the interface eight days before concrete casting. The MB700 was applied only minutes before casting to reduce the period of air contact and, thus, a greater risk of aerosol formation.

All the concrete joints had a curing time of 14 days before testing, corresponding to the concrete achieving 80-90 % of its strength, according to Jacobsen [33]. This was assumed to be sufficient strength for determining adhesion bonds for the different separating actions. During the entire curing period, the specimens were stored at room temperature around 21 °C.

5.1.2 Test setup

The experiment was conducted using the test rig illustrated in figures 5.3 - 5.6 with the following equipment:

- Cantilever strut stand
- Foundation steel plates with toothed surface
- One thick steel plate measuring 20x150x150mm
- One steel dowel pin measuring Φ 10mm/40mm
- Two pieces of cloth
- One steel weight plate of 20 kg

The cantilever strut stand was used to measure the height of the release point. The foundation steel plates made the grouted joint cantilever and more responsive to pure shear failure. The steel dowel, positioned below the thick steel plate, is intended to direct the force towards the connection between the HCS and the joint to provoke a clean shear failure. To achieve this, the two pieces of cloth were placed to keep the thick steel plate at an approximately horizontal level before the impact to direct the resultant force towards the dowel.



Figure 5.3: Test rig

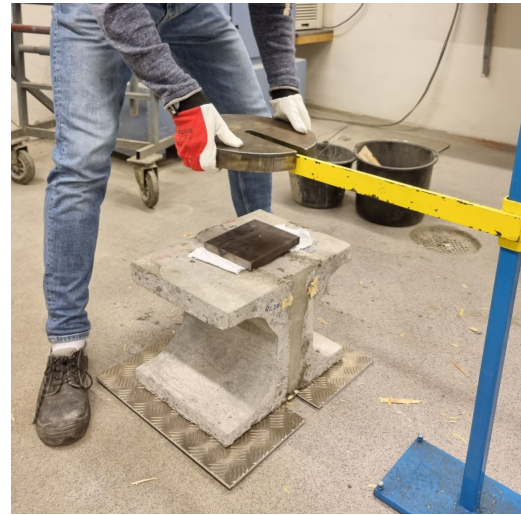


Figure 5.4: Weight plate position



Figure 5.5: Location of steel dowel and rags



Figure 5.6: Steel plate foundation

5.1.3 Collection of data

The experiment was conducted to simplify the disassembly of the longitudinal joint in HCS. As stated in the description of today's disassembly process in Section 4, the first step involves a construction worker using a digging bar or jackhammer to separate the joint. To recreate this process in the first laboratory experiment, the steel dowel represents the tip of a digging bar or jackhammer. It was considered to drop weights on top of a digging bar, but this method was neglected due to HSE factors linked to the high altitude of the weight plate impact.

A weight plate of 20 kg was dropped from varying heights. Each test started from 20 cm above the thick steel plate and had the following successors:

20 cm – 40 cm – 60 cm – 80 cm – 90 cm – 100 cm

After every impact, all covering equipment was removed and a thorough visual examination was conducted to determine if there were any visual cracks or other damages. If a crack was detected, it was attempted to separate the two HCS by hand. Figure 5.7 illustrates an example of such a crack. If manual separation was impossible, the weight plate was dropped again from the same height that induced the crack. This process was repeated until manual separation was possible.

When the grouted joint was separated from one of the HCS interfaces, the residual joint was completely detached from the second HCS by applying several blows with a claw hammer. Figure 5.8 illustrates an example of a residual joint. This part of the experiment is less objective and reproducible due to several variables and was mainly carried out to increase the knowledge of the respective separating action.



Figure 5.7: Crack has occurred



Figure 5.8: Residual joint after separation

5.1.4 Sources of error

As mentioned above, the separating actions were applied 8 days before the concrete was cast. Problems with the concrete proportions due to small aggregate size led to multiple samples with segregation and issues regarding castability, delaying the casting process. The effect of the separating action could differ depending on how long it was in contact with the concrete before casting the joint. Most of the HCS with formwork oils had a dry surface after 8 days, which could impact the friction on the surface. This means the oil evaporated, reacted, or infiltrated the concrete. The effect of a significant time gap between the application of separating actions and the casting procedure is still being determined. However, assembly delays of the HCS on the construction site are common and could lead to varying time gaps. A closer study of the time effect on the separating actions needs to get a comprehensive understanding.

The test setup was very reliant on human actions, which increases the sources of error significantly. The height was measured manually with a measuring tape, and the weight was dropped by hand,

as Figure 5.4 shows. Small errors regarding the dropping height, unequal release, and different angles on the weight plate during an impact - could affect the results.

The test setup simulated disassembly methods used in current practice to provoke a crack. The weight dropped on the cylindrical steel dowel was supposed to imitate the practical disassembly processes used today. This is a significant simplification. However, the objective of this simulation was to determine which separation actions gave the least adhesion bond, and this was possible to obtain without an exact simulation.

The weight and height intervals used in this experiment were determined intuitively, based on the weight of a digging bar and the physical range of hand movements. However, these assumptions are a potential source of error. The height intervals were decided intuitively to have 20 cm steps up to a height of 80 cm, followed by steps of 10 cm up to a height of 100cm. This is an inconsistent choice of intervals and should be reconsidered if the experiment is to be repeated. However, moving from 80 cm to 90 cm was considered sufficient to induce cracks in the samples yet to crack. Furthermore, the safety aspect came into consideration, as the release of weights from large heights could pose a hazard to the personnel involved in the testing process. Therefore, it was important to maintain safety throughout the test and comply with the HSE guidelines set before testing.

5.2 Second laboratory experiment; shear stress transfer

The second part of the laboratory experiment and the second part of the methodology Chapter - has the following hypothesis:

To what extent does the implementation of separating actions between hollow core slabs and their associated longitudinal joints impact the shear capacity through adhesion bond and friction in a laboratory experiment

A shear displacement test was intended to determine the shear capacity of joints applied with separating actions. The measured shear stress represents the ability to transfer shear stress between the joint and HCS and will be referred to as the shear capacity. The agents that gave the least adhesion in the first laboratory experiment from section 5.1 was taken to further testing. This gave four separating actions to study closer, in addition to dry reference specimens:

- **MasterFinish RL 224**

A yellowish vegetable-based formwork oil. The oil is environmentally friendly and can be applied using a paintbrush or a pressure spray. For easy appliances, the intrinsic temperature should be over 0 °C [34].

- **MasterFinish FW 324**

A white chemical form wax. Recommended to apply with a brush or a cloth. However, due to the firm consistency, it is rather challenging to evenly distribute the wax on the surface.

Consequently, it is recommended to develop new application methods for more efficient use on concrete surfaces. Applied with a thick paintbrush in the laboratory test. The surface is visually covered by a thick layer of wax after the appliance. Usable in temperatures down to -15°C , given an intrinsic temperature above 0°C [35].

- **Maapeform W 100**

A white and easy-flowing liquid form wax. The liquid is sprayable, which prevents it from running down vertical surfaces. After spraying, it takes approximately 10 minutes to dry and leaves a thin, invisible wax film on the sprayed surface. Obtains the roughness of concrete surfaces. The liquid is water-based and needs to be protected from frost. Drying time increases with lower temperatures and can not be used in conditions below 0°C [36].

- **Olive Oil**

Regular vegetable olive oil for cooking. Bought from a conventional grocery store, more specifically at Rema 1000. Applied using a pressure spray. Thickens at low temperatures, lumps are formed below 0°C .

- **Dry**

A clean and dry HCS surface to determine the capacity of traditional joints. No separating action applied.

None of these four separating actions contains poisonous aerosols, which makes them convenient to work with.

5.2.1 Test components and material properties

In contrast to the first laboratory experiment, the cut-off HCS were reduced in size and the teething was removed, as Figure 5.9 illustrates. This was done to generalize the resulting shear capacity, regardless of the height of the HCS.

Formwork was built simply with cardboard and duck tape, as Figure 5.10 shows. This was a simple and efficient alternative to the traditional construction of plywood formwork. The testing surface was positioned horizontally, and 20 mm of joint concrete was cast on top, as Figure 5.11 illustrates. To obtain full strength, a minimum of 28 curing days was established. This contrasts with the first laboratory experiment, which only had 14 curing days.

In contrast to the first laboratory experiment, all separating actions were applied using a paintbrush. This method was considered more convenient since the second test only involved one HCS cut-off, and the practical implementation of separating actions had already been explored in the first laboratory experiment. The separating actions were applied one day prior to testing, in contrast to the eight days of delay for casting in the first laboratory experiment. Consequently, some of the surfaces were still slightly moist when casting.

The concrete recipe remained unchanged from the first test. However, due to a delivery issue of Norcem Standard Cement FA CEM II, it was substituted with Norcem Construction Cement FA CEM II. According to Norcem, Construction Cement has a slower hardening rate than Standard Cement FA, but its strength after 28 days should still be comparable [37]. Concrete technologists were consulted to ensure that the changed cement type would not affect the results.

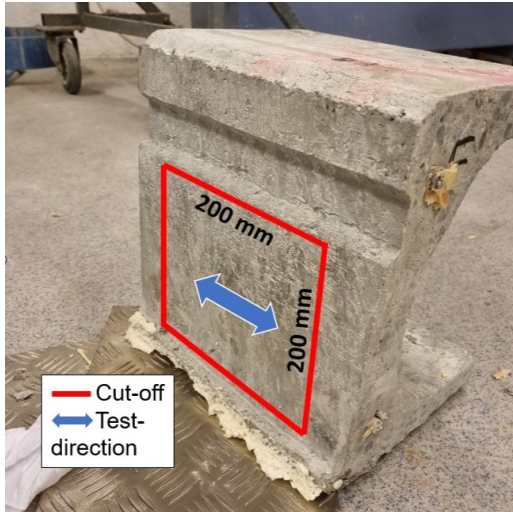


Figure 5.9: Illustration of cut-off on HCS with measurements

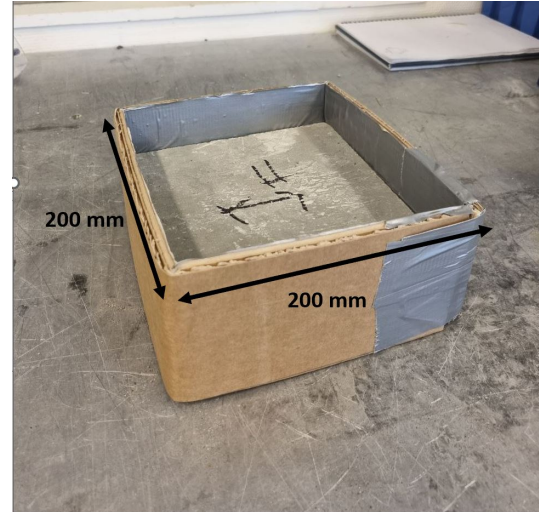


Figure 5.10: HCS sample with formwork and measurements



Figure 5.11: Cast HCS sample with measurements



Figure 5.12: Formwork after leveling and tightened with a ratchet strap

5.2.2 Test setup

A compression machine conducted the shear capacity experiment at the laboratory of NTNU. Deformation, vertical load, and horizontal load were tracked during the test. The horizontal

load was set to a constant value at the start of the test. For fracture tests, constant vertical displacement is best suited due to the control of movements. In contrast, vertical load as the variable will often, upon collapse, damage the setup and specimen, making observation of fractures and cracks impossible. Therefore, the vertical displacement was chosen as the variable, with a constant deformation of 0.02 mm/sec. The machine tracked the necessary force to maintain the given deformation rate throughout the test. The resulting data set gave load values from the horizontal and vertical load cells per deformation.

To mitigate the effect of the irregularities on the outside surface of the concrete, a layer of soft chipboard was positioned on each side of the sample. Subsequently, the concrete sample was positioned between two steel plates to create uniform compression over the joint surface, as Figure 5.14 shows. In order to minimize friction, thin layers of teflon were inserted between the chipboard and the steel plates. Arising friction between the sample and the steel plates could influence the friction capacity of the joint, potentially affecting the accuracy of the obtained data. Moreover, the same friction could lead to a loss of symmetry in the rig setup, leading to a changed attack angle for the vertical shear load.

To monitor the horizontal compression force during the test, a load cell was placed between the right steel plate and a third steel plate; see Figure 5.14. These three plates were tightened with metal struts to create a constant horizontal force. Metal struts were positioned in each corner of the steel plates and tightened evenly with nuts to secure uniform tension load on the sample and to maintain symmetry in the rig.

Due to eccentricity between the support and the vertical force, a bending moment could occur. As this will affect the shear capacity, the eccentricity was reduced to a minimum in order to obtain negligible moment forces in the concrete. If placed centrally on the joint concrete, the vertical load cell was too wide to avoid collisions with the steel plate. Therefore, the setup was switched compared to what was planned, so the vertical load cell attacked the HCS cut-off, while the steel support attacked the joint concrete. Figure 5.14 illustrates the final test setup.

The compression machine has an integrated load cell with a capacity of 400 kN. According to EC2 10.9.3(12), the longitudinal HCS joints have an average maximum shear capacity of 0.15 MPa, equivalent to a maximum point load of 6 kN for the load cell [17]:

$$P_V = 0.15 \frac{N}{mm^2} \cdot 200 \text{ mm} \cdot 200 \text{ mm} = 6000 \text{ N} = 6 \text{ kN} \quad (5.1)$$

Capacity along the joint varies, and 0.15 MPa is based on average shear capacity along the joint. Therefore, the experiment will experience values surpassing 0.15 MPa and 6 kN. Staff at the laboratory advised the measured force to be at least 5 % of the maximum capacity of the load cell's maximum capacity to ensure sufficient data gathering accuracy. However, a load of 6 kN only utilizes 1.5 % of the machine's capacity, meaning that a smaller load cell of 50 kN is necessary to maintain sufficient accuracy. A 50 kN load cell was positioned between the concrete specimen

and the bigger 400 kN load cell. This is illustrated in Figure 5.13. As described in section 5.2.3, the first two samples indicated that the dry surface would reach shear values surpassing 50 kN. Therefore, the dry samples were tested with the 400 kN load cell.

As presented in Section 2.7, the longitudinal joints have a maximum shear capacity, v_{Rdi} , of 0.15 MPa, according to EC2. Section 2.7 also determines the friction coefficient, μ , to be 0.6. Assuming a friction coefficient of 0.6 and an average maximum shear capacity of 0.15 MPa, the correlating normal compression stress, σ_n , is determined as:

$$\sigma_n = \frac{v_{Rdi}}{\mu} = \frac{0.15}{0.6} = 0.25 \text{ MPa} \quad (5.2)$$

Which is equivalent to a normal compression force of 10 kN:

$$P_H = 0.25 \frac{N}{mm^2} \cdot 200 \text{ mm} \cdot 200 \text{ mm} = 10\,000 \text{ N} = 10 \text{ kN} \quad (5.3)$$

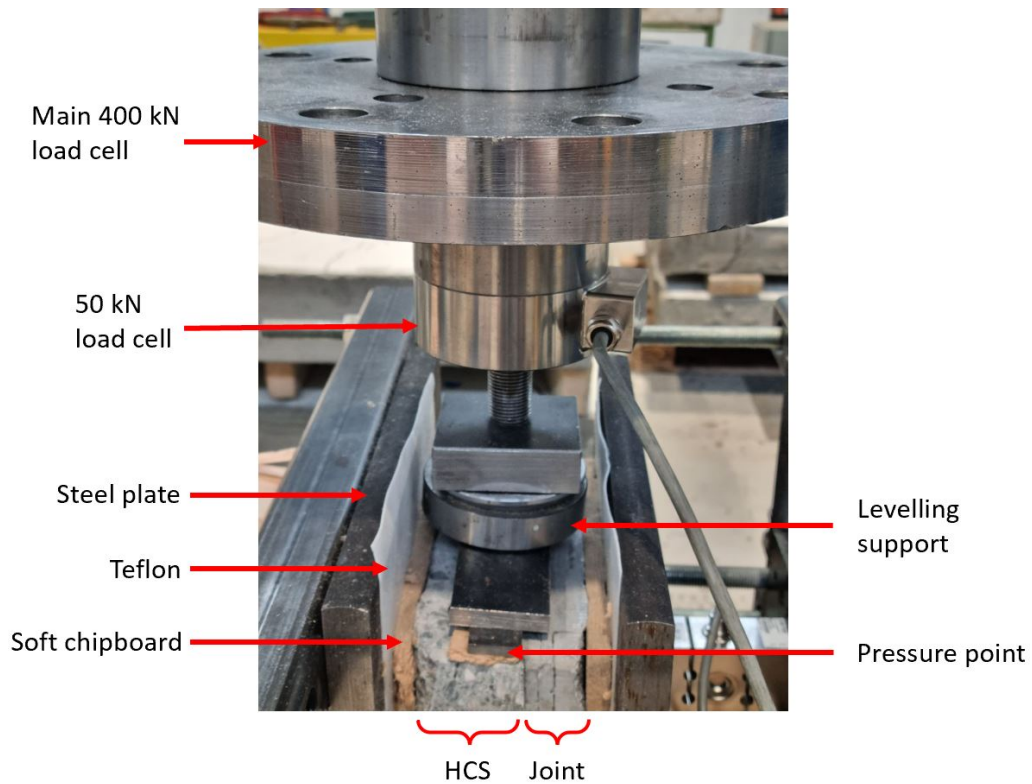


Figure 5.13: Test setup with description

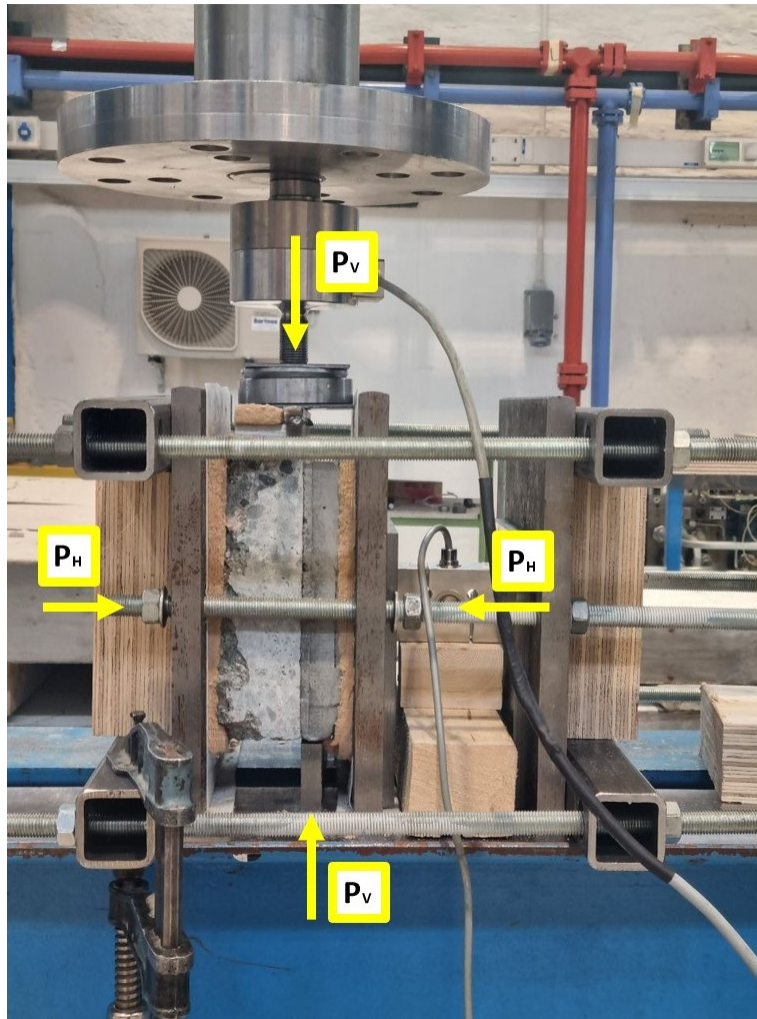


Figure 5.14: Overall view of test setup with acting forces

5.2.3 Collection of data

As for all studies, an increased number of tests increases the accuracy of the study. However, due to time and capacity limits at the laboratory, four tests for each separating action was the highest amount of tests possible. Average values can be determined from the four tests. If one individual test should fail, the test could be dropped from the study while still having three reference values to strengthen the validity of the results. As mentioned, five different surfaces were tested for shear capacity. This gave in total 20 samples for the shear test. Additionally, two extra samples without separating actions were cast to test the rig and setup prior to the official experiment. Therefore, 22 cut-off HCS with joint concrete was cast in the laboratory.

5.2.4 Data processing

The output of the shear test was in the form of text files (.txt) containing empirical data that captured the variables of shear force [kN], normal force [kN], and displacement [mm]. The data was recorded with a minimum precision of one hundredth, and each variable consisted of approximately 6000 to 9000 data points. To convert the forces from kilonewtons (kN) to megapascals (MPa), they were divided by the corresponding surface area. Python codes were utilized for data visualization, enabling the results to be analysed and presented.

5.2.5 Sources of error

As mentioned in section 5.2.1, the cement had to be changed due to failed deliveries to the laboratory. A different cement type can affect the material properties of the concrete. However, it was approved by concrete technologists and should not affect the test results significantly.

Significant variance in adhesion was observed during the rigging of the concrete samples. Two samples with separating actions achieved separation and fell apart before testing. This indicates that the contribution from adhesion on the shear capacity would be zero for these samples. The two concrete pieces were assembled before being rigged into the test setup. When assembled together there is a possibility for restructuring of aggregates and deviating placement.

Maintaining a horizontal load of 10 kN proved challenging, as the load was manually applied tightening nuts on metal struts with spanners. Gradually, the compression force decreased over time due to the loss of tension in the metal struts. As a result, a variance of 0.5 kN could occur between the tests.

The angle of the vertical force applied was determined through manual installation, leading to minor variations. Slender metal plates were placed between the sample and the vertical load cell to direct the forces as close to the joint as possible. However, this configuration was not stable, and there was potential for a slightly skew attack angle. The angle was maintained with reasonable accuracy. However, a small angle can affect the resulting capacity slightly.

6 Results

This section presents a comprehensive analysis of the data obtained from shear testing of longitudinal joints. The results will be separated into two parts, the adhesion test from the first laboratory experiment, followed by the shear capacity test from the second laboratory experiment. Key observations and results will be highlighted in the following chapter, while further data from the tests can be found in Appendix A.

6.1 First laboratory test; adhesion test

6.1.1 Concrete properties

During concrete casting, there is a standard procedure to test the concrete properties. Fresh concrete characteristics such as slump level, density, water-cement ratio, and air content are tested. The concrete recipe used in this experiment is not publicly available, due to it originating from a private company that wishes to maintain its confidentiality, and is therefore not shared in this master's thesis. The results of the fresh concrete tests are shown in Table 6.1.

Table 6.1: Material properties in the first laboratory experiment

Concrete properties			
Slump Level	Density	w/c ratio	Air content
230 mm	2228 kg/m^2	0.40	7 %

After cubical testing of the concrete, the compressive strength, σ_c , was found to be 71.3 MPa. As concrete strength in EC2 is referred to as cylindrical strength, the results were translated using L'Hermite's equation [38]. This gave a ratio of 0.87 between cylindrical and cubical strength. This gave a cylindrical strength of 62 MPa. Converted to strength classes of concrete from EC2 Table 3.1 [17], the concrete can be classified as B60 concrete.

The compressive strength is important in order to determine the crack plane and friction model of the shear test. As the friction models have upper limitations for the compressive strength of the concrete, it is necessary to verify that the strength is below that threshold. The compressive strengths are shown in Table 6.2.

Table 6.2: Compressive strength of concrete in the first laboratory experiment

Compressive strength (σ_c)			
Cubical	Cylindrical	Concrete class	L'Hermite's Ratio
71.3 MPa	62 MPa	B60	0.87

As the results in Table 6.2 show, the concrete has a very high strength. According to the concrete company that provided the concrete recipe, it was intended to produce B35 concrete. However, the obtained strength proved to be around twice the expected strength. Nevertheless, the strength is below the limit of 65 MPa from Walraven’s aggregate interlock model from section 2.5.

6.1.2 Grading of adhesion

The adhesion between the joint and HCS, determining the necessary forces to induce cracks in the joint, will be presented below. The experiment where the joint is being subjected to an impact force from a weight dropped onto a steel dowel pin positioned parallel to the joint, is previously described in section 5.1. Results from this test are shown in Table 6.3.

Table 6.3: Resulting heights before failure and description of the concrete

Adhesion test		
Name	Height at failure	Description
Plastic	20 cm	Very smooth interface. No sign of the degradation of plastic.
MasterFinish RL 224	60 cm(2 drops)	Smooth interface.
Olive oil	60 cm(2 drops)	Crack occurred at first drop. Separation at second drop.
Mapeform W 100	60 cm	Brittle crack fracture. No signs of traces from the agent.
MasterFinish FW 324	80 cm	Interface contains leftovers of the wax.
Water	80 cm	Smooth interface.
Mapeform MB 700	80 cm	Possible chemical influence on the concrete surface.
Mapeform Eco Oil 700	90 cm	Smooth interface. Good cohesion.
Mapecure 1	No Value	Very good cohesion. Joint concrete crushed before separation.
Dry	No value	Very good cohesion. No crack or separation.

Table 6.3 displays the heights of failure for the joints. Instances where there was no separation between the joint and HCS after a drop from 100 cm, are denoted as "No Value". This applied for two of the specimens, where the joints were further attempted removed using a sledgehammer. For both, crushing of the joint or HCS occurred before separation. Appendix A shows pictures of the failure modes and surfaces after separation.

After separation occurred from the weight drop, the residual joint was removed from the remaining HCS using a claw hammer. Intentionally, as previously stated in the section 5.1.3, this final removal of the residual joint was carried out to increase the knowledge of the respective separating action, but without the intention of being a part of the main result. Nevertheless, the number of blows can be found in Appendix A. Subsequently, the surfaces of both the HCS and joint were visually examined to increase understanding of results and used to predict how the separating actions potentially could affect the friction in the second laboratory test. The most significant visual

observations are presented in Table 6.3 in the 'Description' column, and the full overview with pictures is presented in Appendix A.

6.2 Second laboratory experiment; shear capacity

This section provides a presentation of the results from the shear test conducted in the second laboratory experiment. For a detailed description of the test procedure, see section 5.2. The results of the four separating actions and the dry reference are presented in the form of plotted graphs. These graphs illustrate the shear stress-displacement curve for each test along with the corresponding normal stress curve. The measured stress represents the ability to transfer shear stress between joint and HCS, and will be referred to as shear capacity. The first axis represents the displacement in millimetres, while the second axis represents stress in megapascals. The peak value of the stress-displacement curve is visually highlighted in the plot with a red dot and its corresponding value.

A common characteristic found in all plots is the impact of the dowel effect, which is previously described in section 2.6. This effect leads to a slight decrease in the normal stress before rapidly increasing at the same displacement value as the peak shear capacity. Subsequently, the normal stress either increases or remains relatively constant after the initial 'jump'. It is important to emphasize that the displacement was maintained constant throughout the test at a velocity of 0.02 mm/sec. In addition, the shear capacity of all tests reduces gradually in the frictional phase for an increased slip. As described in section 2.5, this is due to further crushing of the irregularities which polishes the surface gradually.

6.2.1 Dry

First, the reference specimen without any separating actions was tested. Figure 6.1 displays the shear capacity of the joint and corresponding normal stress as a function of the displacement. Initially, the stress increases rapidly with increasing deformation until it reaches a peak stress value. Beyond the peak stress, there is a significant drop in stress representing a brittle fracture/slip. Following this drop, the stresses increase slightly before stabilizing at a relatively constant level of around 0.40 MPa. None of the tests dropped below 0.15 MPa, which importance was underlined in section 2.7.

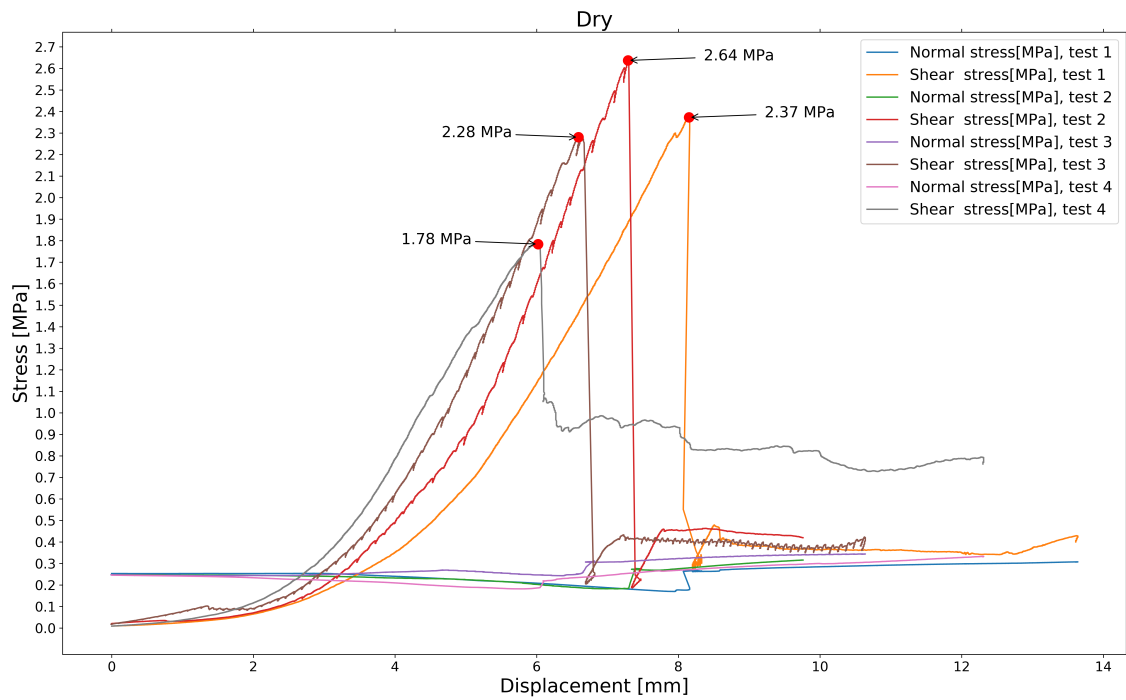


Figure 6.1: Shear capacity of joints without separating actions

Test 4 gave an unusual failure mode of the specimen. After reaching the peak stress, the crack propagated through the HCS, as shown in Figure 6.2. The crack initially propagated along the surface between the joint and HCS, reaching halfway up the joint, where it propagates in a 45-degree direction through the HCS. Due to this failure mode, the test was stopped as the specimen no longer had a complete gliding plane. Consequently, test 4 was excluded from the calculations for the joint capacity. Figure 6.3 shows the specimen for test 4. It is evident that half of the HCS cut-off is detached, while the remaining part still is firmly connected to the joint by a strong adhesion. Notably, the adhesion between the concrete surfaces was stronger than the HCS itself.

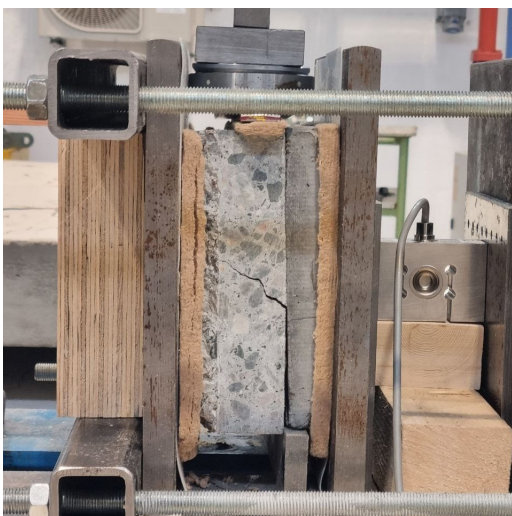


Figure 6.2: Induced crack through the HCS



Figure 6.3: The specimen after testing

6.2.2 MasterFinish FW324

Figure 6.4 shows the shear capacity of the specimens treated with the form wax MasterFinish FW324. In contrast to the other separating actions, the specimens treated with FW324 did not exhibit a clear maximum peak followed by a significant drop. This indicates a negligible contribution from adhesion. The capacity in the friction phase just after failure appears to converge against approximately the same values. Examination of the surface after the test revealed an oily and slippery surface, with clear traces of the form wax present, see Figure 6.5.

The specimen for test 2, with the shear capacity indicated by the red line, had an already detached joint before the start of the test. Separation occurred during the process of lifting the specimen onto the test rig. Although the separation implies no residual adhesion, the specimen has a relatively similar development compared to the other specimens. This can indicate a negligible adhesion for all of the specimens applied with FW324. Shear capacity in the friction phase goes lower than 0.20 MPa for all specimens.

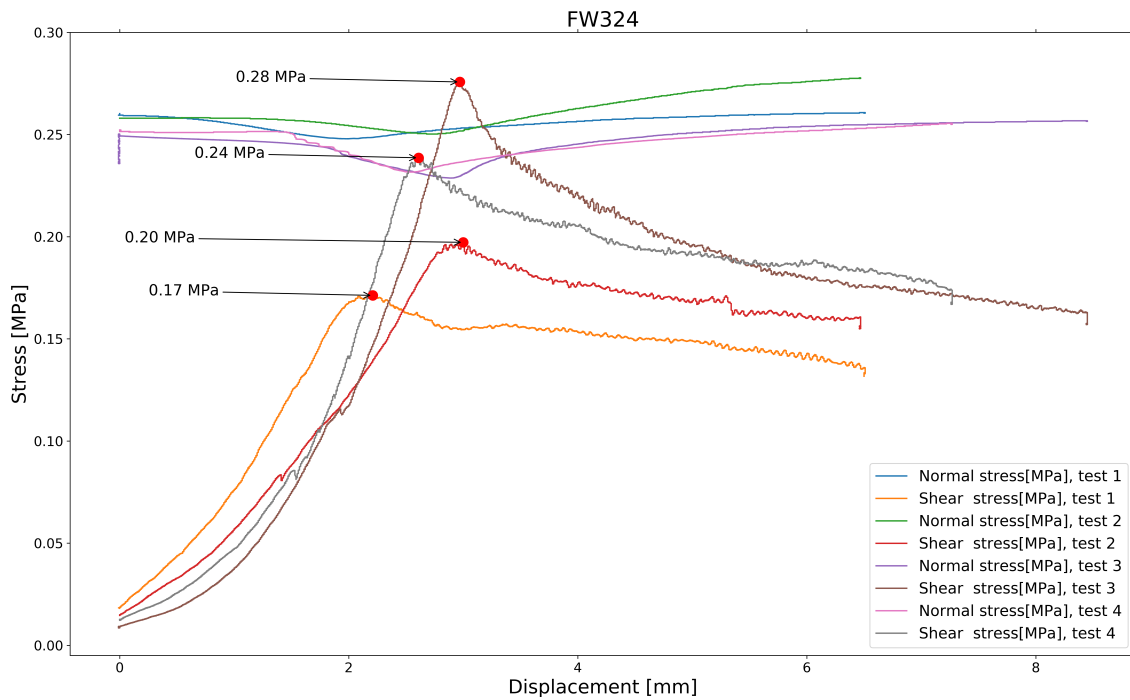


Figure 6.4: Shear capacity of joint applied FW324



Figure 6.5: Surface of specimen applied FW324. Oily and slippery surface

6.2.3 Olive Oil

The results from four tests conducted on specimens treated with olive oil are presented in Figure 6.6. The initial three tests provided relatively similar results. Considering the statistical value, a reliable estimate of the mean stress and interpretations could be derived from these tests, allowing the last test to be utilized to study other aspects. Since the compressive stress on longitudinal joints can vary significantly in reality, and is dependent on numerous factors, it was decided to examine the impact of reduced normal compressive stress. As illustrated in Figure 6.6, the normal stress in test 4 was halved compared to its original normal stress. Consequently, the shear capacity in test 4 was correspondingly reduced to approximately half of the value observed in the initial three tests.

The initial three tests achieved the exact same peak stress capacities. All three tests displayed a settling phase during the build-up before slipping occurred. Additionally, there was a brittle slip down to approximately 0.30-0.35 MPa. Moreover, the friction phase for all three specimens showed a correlating pattern and converged to approximately the same value, with the capacity never surpassing 0.15 MPa. However, it would probably surpass if the displacement range for this experiment was expanded.

In contrast, test 4 has a more irregular trend in terms of capacity. Obtaining the spot where there is an increase in normal stress and assuming it represents the main slip, it does not represent the same displacement value as for the maximum peak stress capacity of 0.19 MPa. Determining the location of the friction phase is harder for test 4.

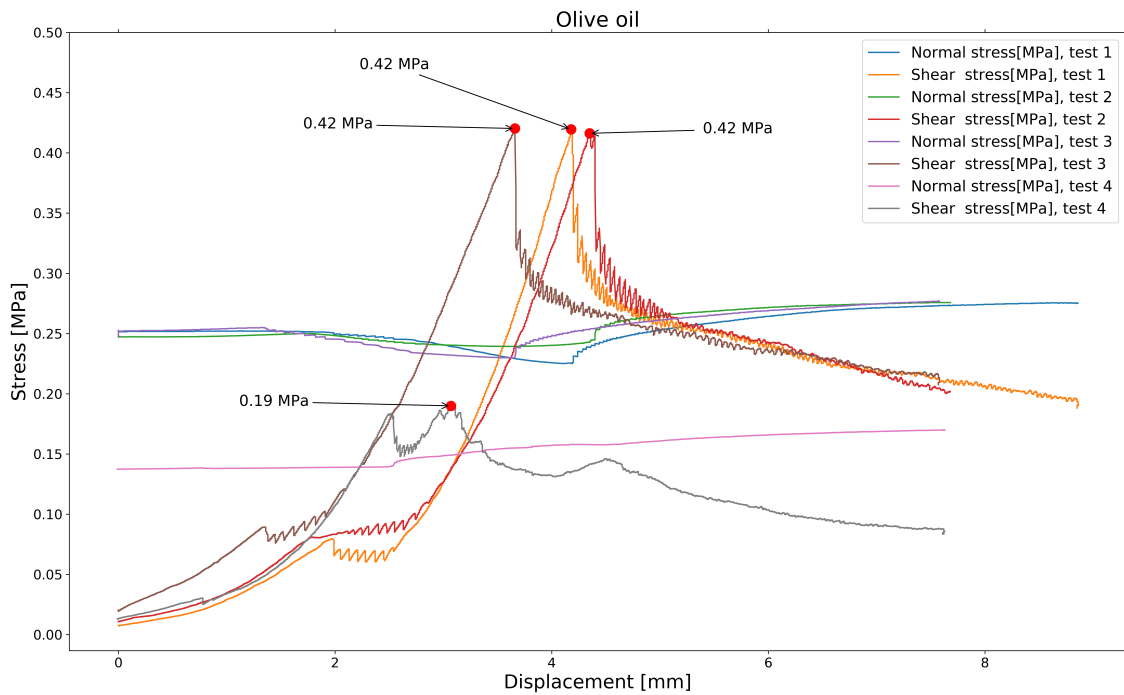


Figure 6.6: Shear capacity of joint applied Olive Oil

6.2.4 MasterFinish RL224

Figure 6.7 shows the shear test results obtained for the vegetable oil MasterFinish RL224 provided by Master Builders Solutions. As the graph shows, there was a large variation in capacity for these specimens. Notably, during test 1, indicated by the yellow line, there were multiple drops in shear capacity before it reached the maximum, leading to an overall big displacement before reaching maximum capacity. Furthermore, the maximum capacity for test 1 was relatively low and the graph indicates a ductile slip.

The specimen used in test 2, with the shear capacity indicated by the red line, had an already detached joint before the start of the test. Separation occurred during the process of lifting the specimen onto the test rig. The build-up to the slip did not exhibit a smooth progression, and the specimen experienced losing capacity five times before the slip occurred. This irregular behaviour is likely to be the reason for the reduced capacity compared to test 3 and test 4. Furthermore, the slip in test 2 was brittle, and the capacity stabilizes at approximately 0.30 MPa. However, the capacity in the friction phase was significantly lower compared to the other specimens, as shown in Figure 6.7. Both test 1 and test 2 surpassed the average maximum shear capacity of 0.15 MPa.

Test 3 and test 4 reached the highest capacities followed by a brittle slip stabilizing at around 0.30-0.35 MPa. They also boasted similar gliding capacities.

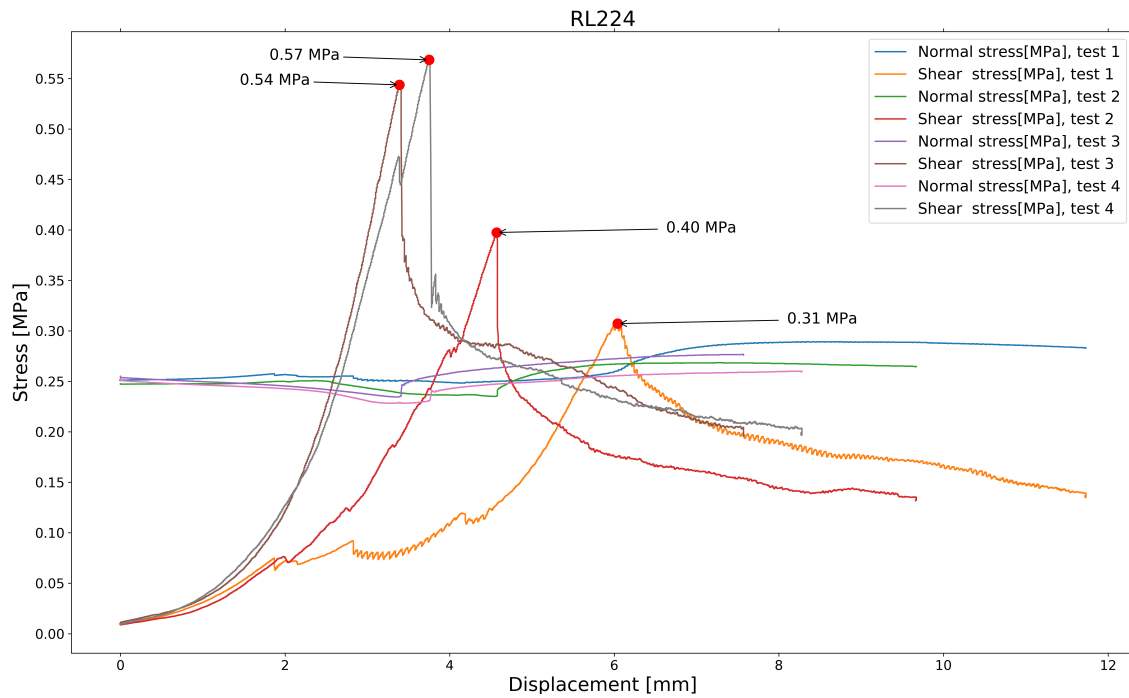


Figure 6.7: Shear capacity of joint applied RL224

6.2.5 Mapeform W100

Figure 6.8 illustrates the shear test results obtained from specimens treated with Mapeform W100, a product provided by Mapei AS. Notably, the Mapeform W100 exhibited a high shear capacity compared to other separating actions. The peak shear capacities had considerable variations. However, the appearance of the build-up phase and the slip mechanism of the specimens, shared many similarities. With the exception of test 4, all specimens exhibited a brittle slip that stabilized at approximately 0.30-0.35 MPa. Additionally, the capacity in the friction phase for all tests, except test 4, appeared to be within approximately the same range of capacity and none surpassed the maximum average capacity of 0.15 MPa.

Due to an error, test 4 experienced only half of the normal stress, approximately 0.125 MPa, compared to the other tests, as shown in the normal stress graph for test 4. As a result, the capacity of the joint was significantly lower and was removed from further calculations.

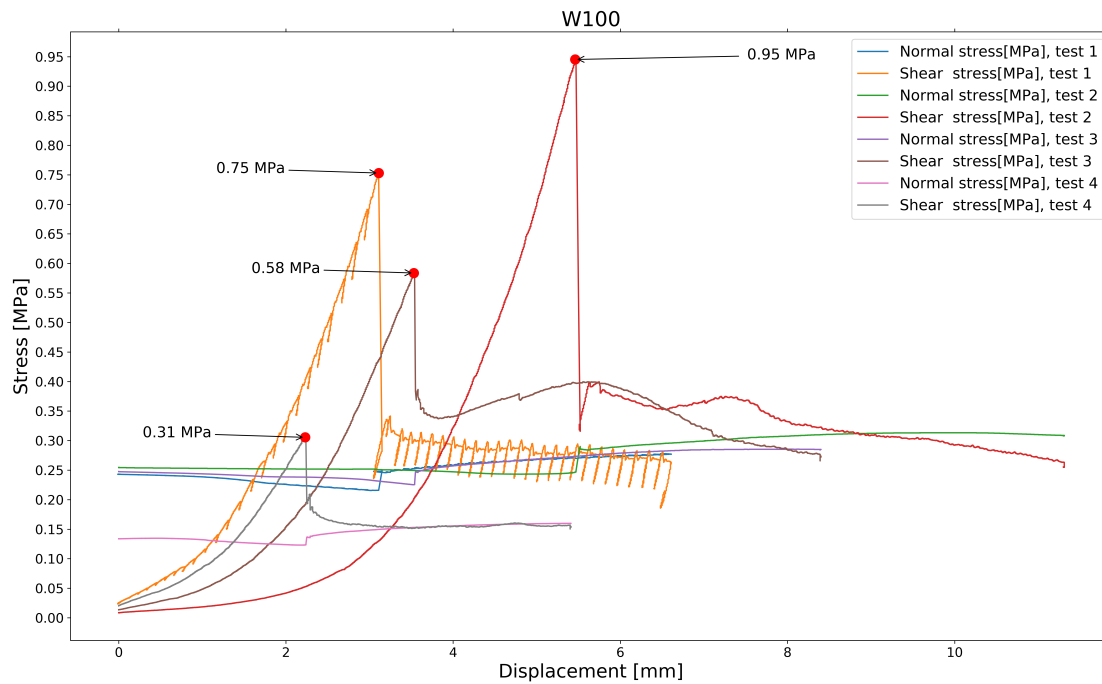


Figure 6.8: Shear capacity of joint applied W100

6.2.6 Results and material properties

Table 6.4 shows the results from the testing of the fresh concrete properties. The results show concrete with high workability from the slump test.

Table 6.4: Material properties in the second laboratory experiment

Concrete properties			
Slump Level	Density	w/c ratio	Air content
240 mm	2242 kg/m ²	0.39	7 %

Table 6.5 shows the material properties of the concrete strength in the second laboratory experiment. Cubical testing of the concrete revealed a cubical compressive strength of 75.8 MPa. The cubical strength was calculated to be 66.5 MPa, using L'Hermite's equation. This can be classified as a B60 concrete, according to Table 3.1 EC2 [17]. Despite a concrete recipe of B30 concrete, the concrete can be classified as B60 concrete.

Table 6.5: Compressive strength of concrete in the second laboratory experiment

Concrete compressive strength (σ_c)			
Cubical	Cylindrical	Concrete class	L'Hermite's Ratio
75.8 MPa	66.5 MPa	B60	0.88

According to EC2 table 3.1, B60 gives the following value for the design axial tensile strength of concrete, f_{ctd} :

$$f_{ctd} = 1.76 \text{ MPa}$$

The upper limit for the shear capacity, $v_{Rdi, max}$, is equal to:

$$v_{Rdi, max} = 0.5 \nu f_{cd} = 0.5 \cdot 0.456 \cdot \frac{60 \cdot 0.85}{1.5} = 7.752 \text{ MPa} \quad (6.1)$$

where ν is determined as,

$$\nu = 0.6 \left[1 - \frac{f_{ck}}{250} \right] = 0.6 \left[1 - \frac{60}{250} \right] = 0.456$$

Assumed *smooth* surface typical for HCS, as described in section 2.7, the adhesion coefficient, c , equals 0.2 and friction coefficient, μ , equals 0.6. From equation 5.2 and the overlaying plots, the normal stress can be found equal to 0.25 MPa. Equation 2.1 provides the following shear capacity, v_{Rdi} , with the given inputs:

$$\begin{aligned} v_{Rdi} &= c f_{ctd} + \mu \sigma_n \\ v_{Rdi} &= 0.2 \cdot 1.76 + 0.6 \cdot 0.25 \\ v_{Rdi} &= 0.352 + 0.150 = 0.502 \text{ MPa} \end{aligned} \quad (6.2)$$

Considering the concrete properties of the joint, the assumption of a *smooth* surface, and the applied normal stress, the shear capacity can be estimated to be 0.502 MPa. It is worth noting that the shear friction contributes 0.15 MPa to the total shear capacity.

As a result of the tests conducted, empirical data is acquired and used in calculations. Table 6.6 shows the average peak- and shear capacity based on the valid tests for each separating action. For peak shear capacity, the dry joints had the highest average peak shear capacity of 2.27 MPa. On the other hand, MasterFinish FW324 had the lowest peak shear capacity of 0.22 MPa.

The friction shear capacity is calculated based on the acquired values from the first part of the friction phase. This refers to the shear capacity in the first 0.5 mm of deformation after the slip has occurred. The average capacity is listed in Table 6.6. The variation in friction shear capacity is notably smaller compared to the peak shear capacity. Dry joints recorded the highest shear friction capacity with 0.40 MPa, while MasterFinish FW324 recorded the lowest value with 0.20 MPa.

Table 6.6: Average peak and friction shear capacity

Average shear capacity		
Separating action	Peak shear capacity [MPa]	Friction shear capacity [MPa]
Dry	2.27	0.40
FW324	0.22	0.20
Olive Oil	0.42	0.29
RL224	0.46	0.28
W100	0.76	0.33

Table 6.7 contains values for the friction- and adhesional coefficient under given conditions. The coefficients are calculated based on equation 6.2 with the same conditions. The friction coefficient is calculated from the friction phase of the shear test, where the adhesion is equal to zero. This gives the following relation for the friction coefficient:

$$\mu = \frac{v_{Rdi}}{\sigma_n} \quad (6.3)$$

The adhesion coefficient is calculated from the peak shear capacity for a *smooth* surface, where the friction coefficient is equal to 0.6. This gives the following relation for the adhesion coefficient:

$$c = \frac{1}{f_{ctd}}(v_{Rdi} - \mu \sigma_n) \quad (6.4)$$

v_{Rdi} , refers to the friction shear capacity from Table 6.6 in the calculation of the friction coefficient, and it refers to the peak shear capacity in the calculation of the adhesion coefficient.

Table 6.7: Friction and adhesion coefficients

Friction and adhesion coefficients		
Separating action	friction coefficient ($c=0$)	Adhesion coefficient ($\mu=0.6$)
Dry	1.6	1.21
FW324	0.8	0.04
Olive Oil	1.16	0.15
RL224	1.12	0.18
W100	1.32	0.35

7 Discussion

The shear transfer is influenced by multiple factors that need to be understood to discuss the obtained results for the solutions proposed in this master's thesis. As stated in section 3.1, Walraven and Reinhardt describe shear transfer across cracks as a complex mechanism, where shear stress, shear displacement, normal stress, and crack width are involved. Consequently, theories from other mechanisms, such as rebar pullout and shear keys in walls, are used to get a comprehensive understanding of the results.

Despite FW324 exhibiting unfavourable characteristics in the first laboratory experiment, it was still included in the second laboratory experiment. The reason behind this decision was to specifically study its shear capacity, considering its smooth surface with residual wax, as observed during the post-test examination of the specimen's surface. The objective was to determine the shear capacity for very smooth surfaces, creating a reference point for low capacity. For the same reason, the dry solution was tested to represent a reference point for high capacity.

However, the plastic film solution was excluded from further testing due to its remarkably low capacity and smooth surface. The thickness of the plastic film hindered the establishment of concrete-to-concrete friction, and was therefore determined to be insufficient for transferring shear forces in longitudinal joints. Nevertheless, the plastic film test revealed that achieving negligible adhesion and friction at the interface is possible.

7.1 Concrete properties

As presented in Chapter 5, the intention was to cast B35 concrete for the shear tests. However, both experiments resulted in grouted joints with compressive strength of B60 concrete, as Table 6.2 and 6.5 show. The high concrete strength requires studying its effect on the shear test results achieved in the second laboratory experiment. As stated in section 2.5, the interlock model of Walraven and Reinhardt is based on the concept of plastic deformation occurring in the weaker matrix surrounding the strong aggregates. The interlock model is examined for compressive strengths up to 65 MPa. While the concrete capacity is slightly below this threshold, the behaviour could be disrupted. In high-strength concrete, aggregates start to fracture through the crack line, which induces a smoother crack surface. This leads to brittle failure, which could reduce the shear resistance and be a partial explanation for brittle fracture observed from many tests. Additional factors affected by the high-strength concrete will be discussed further below.

7.2 Capacity

Looking at the results from section 6.2, it is clear that most capacities following shear slip are higher than the average maximum capacity of 0.15 MPa stated in EC2 10.9.3(12) [17]. The only

exceptions are test 1 for FW324, and test 1 and 2 for RL224. It is reasonable to assume that the average maximum capacity in EC2 includes a safety margin. However, the origin of the theory behind the capacity is unknown, as stated in section 2.7. In addition, it is important to note that this maximum capacity is based on average values, and is allowed to exceed 0.15 MPa in sections along the joint according to the standard.

However, this average maximum capacity of 0.15 MPa is set to be removed in the new revised version of EC2 [25]. The results from the second laboratory test support this decision, as the capacity observed is significantly higher than 0.15 MPa. This can lead to greater utilization of the capacity and encourage engineers to conduct a more thorough investigation of the potential capacity. This can also lead to engineers familiarizing themselves more with the theory concerning shear transfer in joints and relying less on regulations from EC2, which is an important step towards developing new reusable solutions for the joint of HCS.

According to the revised EC2 13.6.2(4) [17], the determination of shear capacity in joints between precast concrete elements without topping concrete should be based on shear-friction mechanisms. This approach differs from the current standard where you are allowed to calculate with a contribution from the adhesion. On the other hand, the approach correlates with current practices where the contribution from adhesion usually is neglected in the calculations due to assumed cracked joints. This revision aligns well with the intention of this master thesis, where the HCS treated with separating actions desirable have negligible adhesion.

When conducting laboratory experiments to evaluate the local capacity of connections in buildings, it is essential to scale the results of small specimens to full-scale global conditions. The shear capacity of a reduced concrete joint may differ from that of a joint on the actual construction site, due to several factors that must be accounted for. Figure 2.16b illustrates the decrease in shear capacity due to an increased joint length. The graph shows a significant reduction in shear capacity for high-strength concrete as the joint length increases. As the laboratory experiment tested the HCS cut-off of 200x200 mm with B60 concrete, it indicates that the capacity would be significantly lower for larger test specimens. As stated in fib 8.4.2.1 [15], this reduction in capacity comes from a lack of stress redistribution upon failure. The concrete tested in the experiment will therefore have a brittle failure, and consequently be more dependent on the length of the joint. Given the high strength of the concrete, full-scale tests need to be conducted to provide a correct estimate of its shear capacity.

A significant trend from the graphs in the results section 6.2, is that the shear capacity is highest for the most fluid agents. At the same time, the thickest waxes generally have lower capacity. This is supported by section 2.5 and 2.6, which underlines the irregularities as the most important factor for both friction and the normal compression force. A very fluid liquid smoothens the irregularities less and maintains better concrete contact. As described in Section 5.2, W100 is an easy-flowing liquid that creates an invisible film on the concrete surfaces. Consequently, an agent like W100

preserves the frictional characteristics of the concrete surface better than the thicker oils, while reducing the adhesion significantly.

7.3 Determination of the contribution from adhesion and friction

As presented in section 6.2, the design shear capacity has contributions from both friction and adhesion. The primary objective of this master's thesis was to analyze various separating actions and investigate their respective shear capacities. In order to gain a comprehensive understanding of the empirical shear capacity, it is essential to examine how friction and adhesion influence the shear capacity. Currently, there is a lack of research providing an overview of how and when friction and adhesion are contributing to shear capacity. Hence, in order to analyze the outcomes, relevant research was interpreted.

Firstly, as presented in section 3.3, research on rebar pullout has determined the shear capacity contribution from adhesion to be dominant at the initial stages with low displacement. Adhesion has been found to exhibit a rigid behaviour, resulting in a rapid increase in capacity with minimal deformation. In contrast, as presented in section 6.2, the RL224 specimen utilized in test 2 detached before the start of the experiment, consequently containing no adhesion.

Assuming that the RL224 specimens utilized in test 3 and test 4 contained a contribution from adhesion, the plot shows a substantial deviation for the tests with and without adhesion throughout all phases of the test. The first phase of the test, with low displacement, shows different gradients for the tests with and without adhesion. This indicates that the adhesion induces a stiffer behaviour in the first part of the shear-slip development. However, the exact phases where adhesion and static friction contribute to the shear slip development are still not fully understood, with previous studies providing different answers.

Furthermore, Figure 6.7 shows some additional variances from the tests of the RL224 specimens. Test 3 and test 4 exhibited a peak shear capacity followed by a brittle slip that stabilizes at approximately 0.30-0.35 MPa. Despite a lower peak- and stabilizing capacity, a similar shear development can be observed for the detached test 2. In contrast, test 1 has a lower peak shear capacity and does not experience a brittle slip afterwards, indicating a more ductile behaviour. The results could indicate that the peak shear capacity of test 2 only relies on the static friction from aggregate interlock. In contrast, test 3 and 4 achieve their peak capacity due to contributions from both adhesion and aggregate interlock. Test 1 never experience a brittle slip in shear capacity, indicating no contribution from adhesion or aggregate interlock, but from dynamic friction in the form of "saw-tooth-shaped interface" friction. The two friction models have previously been described in section 2.5. Although the observations from the tests of RL224 can be used to describe the relationship between adhesion and friction, further tests are necessary to gain a comprehensive understanding.

As presented in section 6.2, the FW324 exhibited the lowest shear capacity, and did not achieve a significant maximum peak or following drop, as Figure 6.4 shows. This indicates that neither effects due to adhesion nor aggregate interlocking have significant contributions to the shear capacity, and indicates that the capacity of the specimen is solely dependent on the gliding friction. Additionally, test 4 of the specimens treated with FW324 detached prior to testing, yet exhibited a similar shear development as the other FW324 specimens. This further proves that treating an interface with FW324 removes the adhesion completely. The development of the FW324 capacities has a similar outlook as Figure 3.7, which indicates no shear keys or static friction from aggregate interlock. Notably, as the concrete surface had obvious traces of the forming wax after testing, it can indicate that the thick layer of wax covers the irregularities and prevents the effect of aggregate interlocking.

7.4 Shear slip relation

As specific shear effects lack comprehensive studies, theory from other shear experiments was used to compare with the shear slip relation observed in this master's thesis. Therefore, section 3.2 presented theory regarding the shear slip relation for a rebar pullout. Interestingly, this shear stress relation has a similar curvature to the results observed in section 6.2. The laboratory test was conducted with smooth concrete interaction, while the rebar pullout utilizes wedging as shear keys, yet it still shows a similar pattern of shear development. Furthermore, the shear slip relationship in walls with shear keys behaves in a similar way as the concrete tested in the laboratory, as stated in section 3.2. Figure 3.7 schematically illustrates the occurrence of a peak shear stress with the presence of shear keys, whereas connections without shear keys maintain a relatively constant shear capacity.

Furthermore, section 2.5 introduces the aggregate interlock mechanism, where local plastic zones lead to the degradation of irregularities and further slip. However, the results from the compressive strength test of the joint concrete reveal an exceptional strength of the concrete, as Table 6.5 shows. The high concrete strength implies that substantial stresses are necessary to generate the plastic zones that facilitate further slip. As a result, according to Walraven and Reinhard, the shear stresses increase significantly. At a certain stress level, the plastic zones occur and a big drop in shear stress will be induced due to the degradation of the irregularities. These mechanisms and observations suggest that the irregularities may exhibit a shear-key behaviour in accordance with the aggregate interlock model. Figure 3.4 shows that a small increase in roughness increases the friction coefficient significantly. This is underlined by Table 6.7 which shows a frictional coefficient significantly higher than 0.6 from EC2 for *smooth* surfaces. Consequently, this could indicate that the concrete surface in the experiments has a larger roughness than expected and that the larger irregularities induce a shear-key behaviour. Further testing needs to be conducted to verify this, but the brittle behaviour could indicate that the concrete strength and roughness affect the results significantly.

7.5 Normal compression forces in the longitudinal joint

As stated in section 6.2, one of the specimens applied olive oil and Mapeform W100, was conducted with approximately 50 % of the standard normal compression stress of 0.25 MPa. As expected, the shear capacity of the specimens decreased significantly in both cases. In the olive oil test, the shear capacity dropped by 55 % from 0.42 MPa to 0.19 MPa, as shown in Figure 6.6. Similarly, in the W100 test, the capacity reduced from around 0.76 MPa to 0.31 MPa, as Figure 6.8 shows, resulting in a capacity reduction of 59 %. These results align with Figure 2.16, which shows the relation between shear stress and normal compression stress for different concrete strengths. This graph demonstrates an approximately linear relationship between shear stress and normal compression stress for uncracked concrete joints. Peak shear capacity from the olive oil and W100 specimens are used to calculate this relation, as the joint has a contribution from adhesion at the peak, indicating an uncracked joint. Furthermore, Figure 2.16 shows that the shear capacity is more affected by the normal compression stress for higher concrete strengths. This correlates with the conducted experiments, where a 50 % reduction in compression force led to a shear capacity reduction of over 50 % for the B60 concrete. These observations support the validity of the laboratory experiments. However, it is important to note that only two tests were conducted with reduced compression stress, which is not sufficient to establish a conclusive relationship for the shear stress.

Figure 2.13 illustrates the mechanism that induces compressive stress on the joint due to the presence of transverse steel, while equation 2.4 shows that the frictional capacity is directly correlated with the compression forces across the joint. However, as modern buildings tend to be designed with longer spans, the distance between transverse reinforcement increases. This could lead to reduced compressive stress in the mid-span of the longitudinal joints. This is crucial to have in mind when designing, to ensure sufficient capacity throughout the entire joint.

7.6 Challenges for reuse

7.6.1 Adhesion

As presented in section 4.2, the demolition project at Lysaker demonstrated that a low adhesion in the longitudinal joint resulted in an efficient disassembly process. However, there have been cases, such as the KA13 project outlined in section 4.1, where strong adhesion caused an ineffective disassembly process. This large variance in disassembly time highlights the challenges regarding the estimation of time and cost for disassembly and emphasizes the need for new solutions in the joint connection between concrete elements to ensure a more predictable process.

Furthermore, as outlined in section 4.2, Mork emphasizes significant advancements in joint work, both in terms of concrete quality and the casting process. Equation 2.4 demonstrates the theoretical correlation between concrete strength and adhesion, while section 2.7 emphasizes that the

workmanship and cleanness of the joint has a significant effect on adhesion between concrete surfaces. Consequently, improved concrete strength, casting process, and cleaning of the HCS prior to casting, could yield exceptional adhesion between concrete elements in modern constructions. As a result, the disassembly time and complexity could increase significantly for future disassembly projects.

The dry specimens, which were not applied with any separating actions in both the first and second laboratory experiments, contributed to the remarkable findings regarding adhesion. In the first laboratory experiment, the joint proved to be impossible to remove from the HCS, despite repeated blows from a sledgehammer. In the second laboratory experiment, the shear capacity was much higher compared to the specimens applied to a separating action, indicating a substantial contribution from adhesion. If the adhesional strength observed in laboratory conditions aligns with the concrete quality and current workmanship at construction sites, future disassembly of HCS will prove highly challenging. There exists a limit to the forces that can be applied for joint disassembly before causing damage to the HCS, thereby removing its reusability.

In the first laboratory experiment, the dry joint exhibited the strongest adhesion compared to the specimen that was watered before casting. As described in section 2.9, the current assembly process involves watering the joint before casting, a practice argued in favour by Mork due to its potential for increasing adhesion. It is therefore interesting that the dry specimen achieved the highest adhesion. Intuitively, watering the joint would remove dirt and potential separating aggregates. However, it is also possible that watering locally affects the concrete during casting, potentially reducing the adhesion between the surfaces. In the laboratory experiment, the HCS cut-offs were already cleaned before testing, reducing the cleaning effect of the water.

As highlighted in section 4.2, Lindseth emphasizes that longer spans of the HCS increase the disassembly time substantially due to the increased contact area of the connection. Equation 2.4 shows the direct correlation between adhesion and the contact area of the concrete. As modern buildings tend to utilize longer spans, the challenge of disassembly could be expected to increase in future projects. Therefore, treating the long-span HCS in each project with separating actions could be particularly relevant.

7.6.2 Logistics

As outlined in section 4.2, Lindseth emphasized the potential for reuse at complex construction sites. This scenario often occurs in urban areas where the demolition site is cramped for space and a tower crane is required to use for the demolition. The process of complex demolishing shares similarities with deconstruction, as concrete elements are frequently handled in the same way. Consequently, the practical, economical, and temporal differences between complex demolishing and reuse are minimal. Therefore, it is advantageous to prioritize projects that offer favourable

conditions for reuse at the start of the development of this executive practice. This approach will improve reuse practices, and increase the amount of reuse projects, which subsequently will reduce cost and time requirements. According to 13.6.2(4) in the revised version of EC2, floors in buildings without topping concrete should rely solely on shear transfer by friction. If the topping layer is thin, the ability to reuse HCS becomes much simpler. Thus, the standard is promoting to only rely on frictional transfer as it facilitates easier removal of connecting joints. Ultimately, regardless of the complexity of the construction site, reuse could be a viable option for all projects.

Additionally, Section 4.2 presents issues regarding the topping concrete on the KA13 project. Letting the topping concrete remain on the HCS still entails that a new topping layer needs to be added. This is because the placement of neighbouring HCS from the previous building does not intuitively correspond to the placement in the new building. Moreover, cutting the edges during the dismantling process may result in an inadequate levelling surface. Furthermore, keeping the concrete cover in the next building would result in a new layer of concrete topping and consequently increase the total weight of the floor. Guidelines for less use of topping concrete or treating the whole HCS with separating actions may be necessary to not significantly change the characteristics of the HCS.

Generally, the cost of reuse projects is the delaying factor for the development and implementation of reuse practices. Section 4.2 addresses the transportation, storage, and design process to be major contributions to the large expenses. To implement an industry change, governmental interventions such as taxation and subsidies are crucial to improve the reuse process. This will lead to more second-hand materials available on the market, combined with an increased focus on DfD-practices. Moreover, the industry will experience more governmental interventions regarding the EU Taxonomy, as presented in section 1.3. The goal of these regulations is to make reuse projects more attractive and profitable for construction companies. However, current cost differences, highlighted in section 4.2, are so significant that stronger regulations may be necessary to fully transform the industry.

7.7 Determination of the best separating action

Based on the current EC2 and the calculation presented in equation 6.2, the specimens tested in the second laboratory experiment are estimated to have a shear capacity of 0.50 MPa. Table 6.6 displays the results, indicating that only the specimen applied Mapeform W100, in addition to the dry joint, exhibited a higher capacity than 0.50 MPa. However, the largest contribution to the shear capacity calculated in equation 6.2 came from adhesion. If calculating with only shear friction transfer, the capacity is equal to the average capacity of 0.15 MPa presented in EC2 10.9.3(12)[17]. In the revised version of EC2, both the condition concerning the average capacity of 0.15 MPa and the opportunity to include the contribution from adhesion will be removed. Consequently, the capacity does not have an upper capacity limit, leaving room for the engineers to utilize the

capacity of the joint better. Therefore, solutions with high capacity are desirable.

From the first laboratory experiment, it was observed that all preferred separating actions fail at 60 cm height. Specifically, W100 fail after only one drop from the weight plate and achieves the greatest peak shear capacity in the second laboratory experiment. W100 is a highly fluid liquid, which quickly is absorbed in the concrete, creating a thin film at the surface. Post-test observations of the specimen support that the thin film does not conceal the surface roughness. Consequently, even with minimal adhesion, the frictional capacity from aggregate interlock is maintained. In addition, as being produced for use on formwork, this form wax has strong resilience against weather conditions at the construction site. Hence, W100 emerges as the preferred separating action for further research. In general, easy-flowing liquids that minimize adhesion are recommended for use on longitudinal joints.

It is important to note that the curing time of W100 increases in colder temperatures, and must be applied on surfaces above 0°C, as stated in section 5.2. This should not be a major problem because the HCS is preheated before casting the joint in cold conditions.

7.8 Sources of error from the results

As the graphs presented in section 6.2 show, the normal compression force in each shear test deviates slightly from 0.25 MPa. This variation occurred because the force was applied manually by tightening nuts. In addition, the compression stress varies within each test as well, indicating a loss of stress from the nuts in the initial stage, and an increase of stress after reaching the peak due to dowel actions from the test setup. As equation 2.2 shows, the shear capacity has a linear relationship with the normal stress during the frictional phase. Consequently, small variances in compression force impact the results significantly.

In section 5.1, it was noted that the casting was delayed by eight days due to issues with the concrete recipe. In contrast, the specimens in the second laboratory experiment were cast the day after the separating actions were applied. Although the casting procedure was different for the two experiments, this variation could serve as a realistic simulation of construction site scenarios where delays in the construction process are common. Implementing the use of separating actions will encourage more research on how the desired action is affected by factors such as weather conditions and pollution.

As mentioned in Section 5.2, the cement had to be changed from Norcem Standard Cement FA CEM II to Norcem Construction Cement FA CEM II in the second laboratory experiment. However, the material properties of the concrete appeared to be very similar for both experiments. A slight increase in the strength from the first to the second laboratory experiment can be explained by a slightly lower w/c ratio for the second test. This is due to the construction cement FA demanding less water than the Standard cement FA. However, the difference is marginal and should

not affect the results between the first and second laboratory experiment significantly.

8 Conclusion and future work

8.1 Conclusion

The revised version of EC2 eliminates the upper limit capacity and provides engineers with the flexibility to fully utilize the capacity of the joint. In combination with the increased emphasis on shear stress transfer through friction in the revised version of EC2, this presents favourable conditions for the implementation of separating actions. The static friction from the aggregate interlock mechanism remains essential for the maximum shear capacity. Therefore, the average peak shear capacity is identified as the key measurement for determining the preferred separating action.

There was a lot of information and knowledge gathered from the results of the specimens applied with RL224. The coincidence regarding the separation of the specimen before testing resulted in valuable insights. While the amount of data is not large enough to confirm the relations, the adhesion appears to be related to the capacity gradient at low displacements and the peak shear capacity. Following this conclusion, the static shear friction consists of a contribution of adhesion and aggregate interlock. The dynamic friction observed in the friction phase is concluded to be a result of the "saw-tooth-shaped interface" theory.

From the results, it clearly emerges that the dry specimens have a significantly higher peak shear capacity. With an average peak shear capacity of 2.27 MPa, the capacity is three times higher compared to W100. However, as indicated by the detached RL224, this capacity gap appears to come from the contribution of adhesion. This contribution is generally neglected in calculations due to assumed cracked joints. Therefore, the peak capacity from the tests of the dry specimens cannot be fully utilized, making solutions with separating actions viable options.

The shear capacity of joints treated with separating actions appears to be correlated to the thickness of the agent. MasterFinish FW324, the thickest form wax, had the lowest shear capacity of 0.22 MPa. The most easy-flowing liquid, Mapeform W100, had a peak shear capacity of 0.76 MPa, while the remaining oils had a capacity in-between. The results show that easy-flowing liquids such as W100 maintain the roughness of the concrete interface, facilitating shear transfer through friction. Additionally, W100 are easy to apply with a spray, while also boasting a strong resilience against weather conditions on construction sites. Therefore, W100 emerges as the preferred separating action due to its highest average peak shear capacity, and favourable practical qualities.

The highlighted challenges regarding the cost of disassembly, transportation and storage make reuse projects more expensive than traditional projects. Therefore, governmental subsidies and taxation are necessary to make reuse projects economically sustainable. This will lead to a gradual increase of reuse projects. As the amount of reuse projects increases, there will be more second-hand materials available, demolishing workers will have more experience in complex disassembly,

and reuse will be better implemented in the design process. Consequently, the time and cost of reuse projects will be reduced.

The significant variance in adhesion from the KA13 project to the Lysaker project highlights the challenging project estimations for demolition contractors. Additionally, adhesion in future joints is anticipated to increase due to improvements in the joint work emphasized by Mork. Furthermore, increased span length will increase the contact area of the concrete, requiring bigger forces to dismantle the joint. Therefore, the reduction of adhesion is crucial to secure a more predictable and effective disassembly process, which further underlines the potential of separating actions.

Overall, the findings of this study provide valuable insights into shear transfer mechanisms, the role of adhesion and friction, and the capacity of concrete joints. The results contribute to the understanding of shear transfer in practical applications and can inform future design approaches and considerations for reuse projects. Further research and experimentation are recommended to expand upon these findings and gain a more comprehensive understanding of shear transfer in concrete connections.

8.2 Future work

8.2.1 External variables

As discussed in 7.2, the capacity was shown to vary significantly based on the joint length. As a result, full-scale tests need to be conducted to determine the shear capacity in actual floorings and roofs.

The laboratory experiment was conducted under controlled conditions with minimal external variables and at room temperature. These conditions vary significantly from the construction site. Further experiments need to be conducted to survey the long-term effects of separating actions. Also, as separating actions are affected by temperature fluctuations, performing tests in various temperatures should be conducted. Lastly, the effect of continuous rain on the surface before casting could be examined.

8.2.2 Laboratory experiment without normal stress

The contribution from adhesion in the second experiment proved challenging, and the best knowledge on adhesion comes from the first laboratory experiment, in addition to failed specimens that underwent separation before testing in the second laboratory experiment. The absence of previous research with similar experimental conditions made the adhesional contribution difficult to estimate. If reproduction of the experiment is to be carried out, it is recommended to allocate more resources to determine the adhesion in the first laboratory experiment. The authors also

encourage conducting shear tests, but without normal stress to isolate shear friction as a variable. This approach aims to increase the understanding of how adhesion contributes to the capacity when separating actions is applied.

Bibliography


- [1] T. Lindseth, *Ombruk hulldekker*, Marius L. Jensen and Isak M. Lamvik, Lysaker/visit at construction site, Mar. 2023.
- [2] E. M. Foundation, “Completing the picture: How the circular economy tackles climate change”, 2021.
- [3] Skanska. “Sirkybygg”. (), [Online]. Available: <https://www.skanska.no/hvem-vi-er/barekraft/miljo-og-gronne-losninger/innovasjon-og-fou/sirkbygg/> (visited on Jun. 5, 2023).
- [4] E. Commission. “About the european commission”. (), [Online]. Available: https://commission.europa.eu/about-european-commission_en (visited on Mar. 3, 2023).
- [5] E. Commission. “Faq: What is the eu taxonomy and how will it work in practice?” (), [Online]. Available: https://finance.ec.europa.eu/system/files/2021-04/sustainable-finance-taxonomy-faq_en.pdf (visited on Feb. 15, 2023).
- [6] H. Engesæth and L. Sjøli, “Taksonomiens innvirkning på bygg- og anleggsbransjen”, *Byggeindustrien*, 2023.
- [7] E. Lov. “Eu-rammeverk for fremme av grønne investeringer: Utfyllende bestemmelser om klassifiseringssystemet”. (), [Online]. Available: <https://www.europalov.no/rettsakt/eu-rammeverk-for-fremme-av-gronne-investeringer-utfyllende-bestemmelser-om-klassifiseringssystemet/id-28551> (visited on Mar. 4, 2023).
- [8] E. Commission. “Circular economy action plan - for a cleaner and more competitive europe”. (), [Online]. Available: https://ec.europa.eu/environment/circular-economy/pdf/new_circular_economy_action_plan.pdf (visited on Mar. 1, 2023).
- [9] N. G. B. Council. “Om breeam-nor”. (), [Online]. Available: <https://byggalliansen.no/sertifisering/om-breeam/> (visited on Mar. 3, 2023).
- [10] N. I. System. “Hollow core slabs”. (), [Online]. Available: <https://www.nordimpianti.com/Concrete-Elements/Hollow-Core-Slabs>.
- [11] Spenncon. “Hulldekk”. (), [Online]. Available: <https://spenncon.no/produkter/hulldekk/>.
- [12] Betongelementforeningen, *Betongelementboken*. Betongelementforeningen, 1995.
- [13] I. B. E. M. Lamvik and M. L. Jensen, “Demonterbare knutepunkt i hulldekker”, *NTNU*, 2023.
- [14] O. S. Hopperstad, *Mechanics 4, Lecture Notes*. NTNU, 2021.
- [15] I. F. for Structural Concrete (fib), “Structural connections for precast concrete buildings”, 2008.
- [16] I. for konstruksjonsteknikk, *Formelsamling TKT4175 Betongkonstruksjoner 1*. NTNU, 2021.


-
- [17] S. Norge, “Ns-en 1992-1-1:2004+a1:2014+na:2018: Eurocode 2: Design of concrete structures - part 1-1: General rules and rules for buildings.”, 2021.
- [18] P. W. Birkeland and H. Birkeland, “Connections in precast concrete construction”, 1966.
- [19] K. Carlsson, “Skjuvningskapacitet hos armerade fogar i betong-konstruktioner”, *Royal Institute of Technology*, 1979.
- [20] J. Walraven and H. Reinhardt, “Theory and experiments on the mechanical behaviour of cracks in plain and reinforced concrete subjected to shear loading”, pp. 26–33, 1981.
- [21] J. X. et al., “Shear-friction behavior of concrete-to-concrete interface under direct shear load”, 2021.
- [22] N. W. Hanson, “Precast-prestressed concrete bridges 2. horizontal shear connections”, *Journal of the PCA Research and Development Laboratories*, n^o2 (May), pp. 38–58, 1960.
- [23] K. Gustavsson, *Joints in composite concrete structures with thin topping*. Chalmers University of Technology, Division of Concrete Structures, 1981.
- [24] B. O. Mork, *Endring av fugestøp*, Marius L. Jensen and Isak M. Lamvik, Forskjell i dagens fugestøp fra tidligere, May 2023.
- [25] S. Norge, “Fpren 1992-1-1:2022”, 2022.
- [26] M. M. et. al, “Friction and cohesion coefficients of composite concrete-to-concrete bond”, 2014.
- [27] L. Xu, T. K. Hai, and L. C. King, “Bond stress-slip prediction under pullout and dowel action in reinforced concrete joints”, *ACI Structural Journal*, vol. 111-S83, 2014.
- [28] E. ASA, “Erfaringsrapport ombruk”, *Entra ASA*, 2020.
- [29] S. Norge. “Hollow core slabs for reuse”. (), [Online]. Available: <https://www.standard.no/no/Nettbutikk/produktkatalogen/Produktpresentasjon/?ProductID=1407012> (visited on May 11, 2023).
- [30] G. van den Brink, “Designing with recovered precast concrete elements”, *A study on the possibilities of reusing structural precast concrete elements, from disassembled office buildings, in new apartment buildings*, pp. 16–22, 2020.
- [31] Ø. Rønningen, “Sirkybygg - årsrapport”, 2023.
- [32] G. e. a. Möller, *Betonghandboken*. Svensk Byggtjänst, 1982.
- [33] S. e. a. Jacobsen, *Concrete technology*. NTNU, 2023, ch. 12, 15.
- [34] M. Builders, “Masterfinish rl224”, *Produktdatablad*, 2021.
- [35] M. Builders, “Masterfinish fw324”, *Produktdatablad*, 2019.
- [36] Mapei, “Mapeform w100”, *Produktdatablad*, 2022.
- [37] N. H. C. Group, “Herdeteknologi”, pp. 4–5, 2022.


-
- [38] D. Elwell and F. Gongkang, "Compression testing of concrete: Cylinders vs. cubes", pp. 21–25, 1995.


Appendix


A Pictures and descriptions from first laboratory test


Separating action	Dry (No separating action)
Height when failure	No value
Residual joint collapse [approximately number of hammer blows]	No value
Picture of failure	
<p>Very good cohesion. The initial testing procedure did not give any crack or separation. Consequently, a large sledgehammer was used to provoke failure which led to separation in parts of the surface.</p>	


Separating action	Mapeform Eco Oil 700
Height when failure	90 cm (x2 drops)
Residual joint collapse [approximately number of hammer blows]	>20 (30)
Picture of failure	
<p>Smooth interface. Good cohesion. Hard to remove residual joint.</p>	


Separating action	MasterFinish FW 324
Height when failure	80 cm
Residual joint collapse [approximately number of hammer blows]	10
Picture of failure	
<p>Smooth interface. MasterFinish FW 324 is a wax-based viscous substance and moisty leftovers was still present during post-collapse observation.</p>	


Separating action	Mapecure 1
Height when failure	No value
Residual joint collapse [approximately number of hammer blows]	No Value
Picture of failure	
<p>Very good cohesion. The initial testing procedure did not give any crack or separation. Consequently, a large sledgehammer was used to provoke failure which led to compression failure in the joint concrete instead of separation.</p>	


Separating action	Mapecure MB 700
Height when failure	80 cm
Residual joint collapse [approximately number of hammer blows]	15
Picture of failure	
<p>Strange surface in the interface. Possible chemical influence from the MB 700 on the concrete.</p>	

Separating action	Olive oil
Height when failure	60 cm (x2 drops)
Residual joint collapse [approximately number of hammer blows]	10
Picture of failure	
<p>Crack occurred at first drop from 60 cm. Repetitive drop was conducted from 60 cm which led to collapse.</p>	

Separating action	Plastic
Height when failure	20 cm
Residual joint collapse [approximately number of hammer blows]	5
Picture of failure	
Very smooth interface. No sign of degradation on plastic wrap.	

Separating action	MasterFinish RL 224
Height when failure	60 cm (x2 drops)
Residual joint collapse [approximately number of hammer blows]	5
Picture of failure	
Crack occurred at first drop from 60 cm. Repetitive drop was conducted from 60 cm which led to collapse. HCS was also damaged by the weight plate bouncing of after impact.	

Separating action	Mapeform W 100
Height when failure	60 cm
Residual joint collapse [approximately number of hammer blows]	20
Picture of failure	
Smooth interface. Very brittle fracture, no sign of cracking before failure.	

Separating action	Water
Height when failure	80 cm
Residual joint collapse [approximately number of hammer blows]	>20
Picture of failure	
Smooth interface. Significant amount of hammer blows to release residual joint.	



 **NTNU**

Norwegian University of
Science and Technology